© 2017. Published by The Company of Biologists Ltd | Development (2017) 144, 2259-2269 doi:10.1242/dev.152231

RESEARCH ARTICLE

The cell wall-localized atypical β-1,3 glucanase ZERZAUST controls tissue morphogenesis in *Arabidopsis thaliana*

Prasad Vaddepalli[1,*], Lynette Fulton[1], Jennifer Wieland[1], Katrin Wassmer[1], Milena Schaeffer[2], Stefanie Ranf[2] and Kay Schneitz[1,‡]

ABSTRACT

Orchestration of cellular behavior in plant organogenesis requires integration of intercellular communication and cell wall dynamics. The underlying signaling mechanisms are poorly understood. Tissue morphogenesis in *Arabidopsis* depends on the receptor-like kinase STRUBBELIG. Mutations in *ZERZAUST* were previously shown to result in a *strubbelig*-like mutant phenotype. Here, we report on the molecular identification and functional characterization of *ZERZAUST*. We show that *ZERZAUST* encodes a putative GPI-anchored β-1,3 glucanase suggested to degrade the cell wall polymer callose. However, a combination of *in vitro*, cell biological and genetic experiments indicate that ZERZAUST is not involved in the regulation of callose accumulation. Nonetheless, Fourier-transformed infrared-spectroscopy revealed that *zerzaust* mutants show defects in cell wall composition. Furthermore, the results indicate that ZERZAUST represents a mobile apoplastic protein, and that its carbohydrate-binding module family 43 domain is required for proper subcellular localization and function whereas its GPI anchor is dispensable. Our collective data reveal that the atypical β-1,3 glucanase ZERZAUST acts in a non-cell-autonomous manner and is required for cell wall organization during tissue morphogenesis.

KEY WORDS: *Arabidopsis*, Cell wall, Glucanase, Receptor-like kinase, STRUBBELIG, ZERZAUST

INTRODUCTION

Tissue morphogenesis depends on cell-cell communication as cells divide and undergo anisotropic growth in a coordinated fashion. In plants, however, the cell wall imposes restrictions on the shape and movement of cells and thus communication of cellular behavior must be intrinsically linked to cell wall biogenesis and dynamics. It is a key challenge in plant biology to understand the mechanistic basis of these signaling processes.

Organogenesis in *Arabidopsis* requires signaling mediated by the leucine-rich repeat receptor-like kinase (RLK) STRUBBELIG (SUB), also known as SCRAMBLED (Chevalier et al., 2005; Kwak et al., 2005; Vaddepalli et al., 2011; Lin et al., 2012). Absence of *SUB* function results in abnormal integument initiation and outgrowth, aberrant floral organ and stem morphology, reduced plant height and irregular leaf shape. SUB signaling further contributes to orientation of the cell division planes in the L2 layer of the floral meristem (FM) and to root hair patterning. SUB is unusual as it represents an atypical or 'dead' RLK. Although its primary sequence is indicative of its conserved family, and SUB requires the presence of the kinase domain per se for function, enzymatic phosphotransfer activity is not essential for its activity *in vivo* (Chevalier et al., 2005; Vaddepalli et al., 2011; Kwak et al., 2014).

QUIRKY (QKY) represents a central component of SUB signaling (Fulton et al., 2009; Trehin et al., 2013; Vaddepalli et al., 2014). Mutations in *SUB* and *QKY* result in similar phenotypes and a large overlap of misregulated genes in flowers. QKY carries four C2 domains, two transmembrane regions in a C-terminal phosphoribosyltransferase C-terminal domain (PRT_C), and localizes to plasmodesmata (PD). PD are membrane-lined channels interconnecting most plant cells and they control intercellular movement of various types of molecules (Otero et al., 2016; Tilsner et al., 2016). Recent data indicated that SUB interacts directly with QKY at PD (Vaddepalli et al., 2014). Moreover, *SUB* and *QKY* act non-cell-autonomously across several cells (Kwak and Schiefelbein, 2008; Yadav et al., 2008; Vaddepalli et al., 2014). As SUB and QKY proteins do not appear to move between cells, it is likely that SUB signaling results in the formation or propagation of an as-yet-unknown *SUB*-dependent mobile signal (SMS).

Mutations in *ZERZAUST* (*ZET*) (German for 'tousled') also result in a strong *sub*-like phenotype during the development of ovules, flowers and stem and during root hair patterning (Fulton et al., 2009). In addition, flowers of *sub* and *zet* mutants are characterized by a similar set of responsive genes. For example, in discrete flower samples at stages 1-9 or stages 10-12, 54% or 81%, respectively, of genes misregulated in *sub* mutants were correspondingly misregulated in *zet* mutants (Fulton et al., 2009).

Glycosylphosphatidylinositol (GPI)-anchored proteins are usually located at the cell surface and are known to regulate a broad range of biological processes (Gillmor et al., 2005; Fujita and Kinoshita, 2012; Yu et al., 2013; Li et al., 2015). Nascent full-length GPI-anchored proteins contain an N-terminal signal peptide and a C-terminal hydrophobic tail, both of which eventually get processed in the endoplasmic reticulum (ER) lumen. Afterwards, a GPI anchor, which is synthesized in the ER is added to the ω site at the C terminus. Subsequently, the mature protein is targeted to the cell surface. As the GPI anchor is susceptible to cleavage by specific phospholipases, these proteins can be localized to either plasma membrane or extracellular matrix (Orlean and Menon, 2007).

Here, we show that *ZET* encodes a GPI-anchored predicted β-1,3 glucanase. The results suggest that ZET localizes to the cell wall and that *ZET* acts non-cell-autonomously, similar to *SUB* and *QKY*. Finally, the data indicate that although ZET affects the chemical properties of the cell wall the catalytic residues of ZET are not required for its function *in vivo*.

[1]Entwicklungsbiologie der Pflanzen, Wissenschaftszentrum Weihenstephan, Technische Universität München, 85354 Freising, Germany. [2]Lehrstuhl für Phytopathologie, Wissenschaftszentrum Weihenstephan, Technische Universität München, 85354 Freising, Germany.
*Present address: Laboratory of Biochemistry, Wageningen University, 6708 WE Wageningen, The Netherlands.

‡Author for correspondence (kay.schneitz@tum.de)

P.V., 0000-0002-9236-6063; L.F., 0000-0002-9640-5840; J.W., 0000-0002-2824-8230; K.S., 0000-0001-6688-0539

Received 16 March 2017; Accepted 4 May 2017

Development (2017) 144, 2259-2269 doi:10.1242/dev.152231

RESULTS

ZET encodes a GPI-anchored putative β-1,3 glucanase

We cloned and identified *ZET* as At1g64760 by map-based cloning, the isolation of multiple alleles and complementation experiments (Fig. 1) (Table S1; supplementary Materials and Methods). ZET was identified in a proteomic screen for GPI-anchored proteins (Elortza et al., 2006) and is predicted to be a β-1,3-glucanase (BG) (EC 3.2.1.39).

ZET belongs to the 50-member BG gene family in *Arabidopsis* (Doxey et al., 2007; Gaudioso-Pedraza and Benitez-Alfonso, 2014). BGs are typically involved in the degradation of callose, a cell wall polymer consisting of mainly β-1,3-linked homopolymers of glucose (Zavaliev et al., 2011). Sequence analysis suggests that the ZET protein carries an N-terminal signal peptide followed by a glycoside hydrolase domain family 17 domain (GH17) and a C-terminal X8 or carbohydrate-binding module family 43 (CBM43) domain (Fig. 1A). GH17 domains typically hydrolyze 1,3-β-D-glucosidic bonds of β-1,3 glucans (Henrissat et al., 2001) and several CBM43 domains are known to bind β-1,3 glucans *in vitro* (Barral et al., 2005; Simpson et al., 2009). The ethyl methanesulfonate (EMS)-induced *zet-1* mutation (L*er* background) is predicted to result in a truncated protein with 88 residues followed by a stretch of 25 novel amino acids (Fig. 1A). The Ds-transposon insertion in *zet-2* (induced in L*er*) is predicted to lead to a shorter protein with 64 residues followed by 45 aberrant residues. The *zet-2* allele is slightly stronger than *zet-1*.

To confirm the identification of *ZET* we performed complementation tests. To this end, we generated a fluorescent protein-based reporter construct. As ZET is predicted to reside at the outer leaflet of the plasma membrane (PM) we made use of T-Sapphire (TS), a pH-stable variant of GFP (Zapata-Hommer and Griesbeck, 2003). TS was inserted in-frame between the signal peptide and the GH17 domain of ZET. The TS:ZET fusion proved to be functional. The *zet-1* plants carrying the *TS:ZET* reporter gene under the control of the endogenous *ZET* promoter (*pZET::TS:ZET*) (see Materials and Methods) or the *UBQ10* promoter (*pUBQ::TS:ZET*) showed a wild-type morphology (*pZET::TS:ZET zet-1*: 38/38 independent T1 lines) (*pUBQ::TS:ZET zet-1*: 25/25) (Fig. 1B-F). Western blot assay confirmed the presence of an intact TS:ZET fusion protein *in planta* (Fig. S1). Thus, the results of these genetic complementation tests confirm the identity of *ZET*.

ZET is expressed in a broad fashion

To assess the *ZET* expression pattern during floral development, we carried out *in situ* hybridization of sectioned floral tissue. Young FMs revealed a very weak but broad signal distribution whereas young ovules exhibited a similarly weak but spottier expression pattern (Fig. 2A,B). To gain further insight into the *ZET* expression pattern, we analyzed plants expressing a β-glucuronidase (GUS) reporter gene under the control of the native *ZET* promoter (*pZET::GUS*). Weak reporter signal was observed throughout the FM (Fig. 2C). During ovule development, the strongest signal was seen in the inner integument (Fig. 2E-G). Reporter activity could also be observed in many tissues including pistils, seedlings, the meristem of the main root, and lateral root primordia (Fig. 2H-M). These results indicate that *ZET* is expressed in a wide range of tissues.

TS:ZET localizes to the apoplast

To assess where ZET is localized within the cell, we investigated the TS:ZET signal localization in our complemented reporter lines. Confocal microscopy revealed nearly identical tissue distribution and subcellular TS:ZET signal localization for *pZET::TS:ZET zet-1* and *pUBQ::TS:ZET zet-1* plants. At the tissue level, detectable signal distribution for both types of TS:ZET reporter lines appeared much more restricted in comparison with the broad signal distribution expected for a pUBQ promoter-driven reporter or

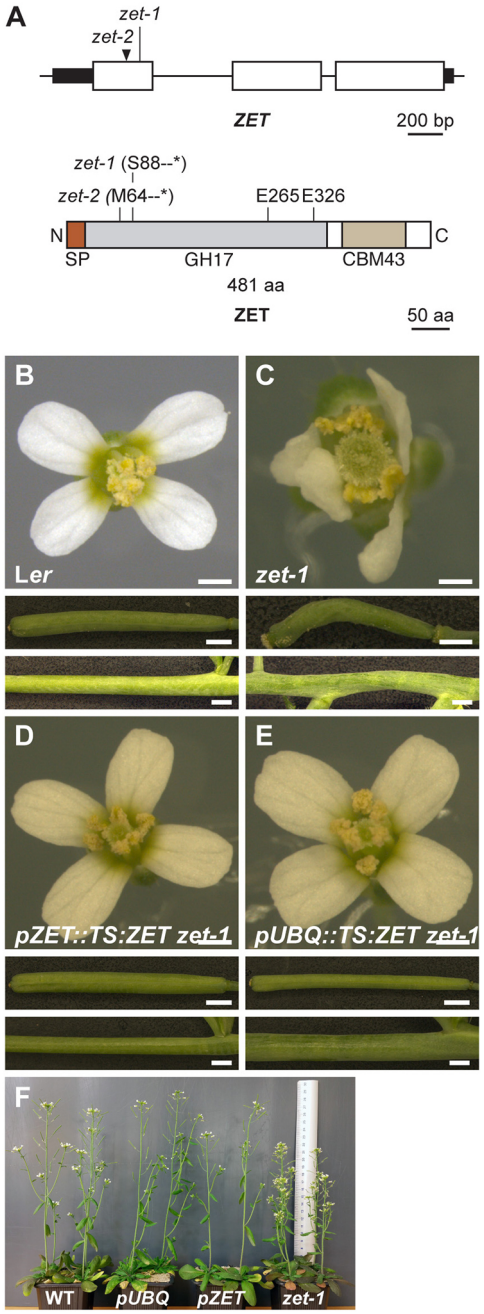

Fig. 1. Molecular characterization of *ZET*. (A) Top: Schematic depicting the genomic organization of *ZET*. Horizontal lines represent introns. Filled rectangles mark untranslated regions. The positions of EMS- (line) and transposon- (arrowhead) induced mutations are indicated. Bottom: Schematic of the predicted ZET protein. The signal peptide (SP) and the GH17 and CBM43/X8 domains are highlighted as are the two catalytic glutamic acids of the GH17 domain. The position and effects of the *zet* mutations are indicated. (B-F) Complementation of *zet-1* phenotype by two TS:ZET reporter constructs. (B-E) Top: Stage 13 flower. Middle: Siliques. Bottom: Stem. Genotypes are indicated. (C) Note aberrant floral morphology. Siliques and stems are twisted. (D,E) Note normal phenotype of *zet-1* plants carrying the respective reporter constructs. (F) Whole-plant appearance. Genotypes are indicated. pUBQ: *pUBQ::TS:ZET zet-1*; pZET: *pZET::TS:ZET zet-1*. Scale bars: 0.5 mm.

Development (2017) 144, 2259-2269 doi:10.1242/dev.152231

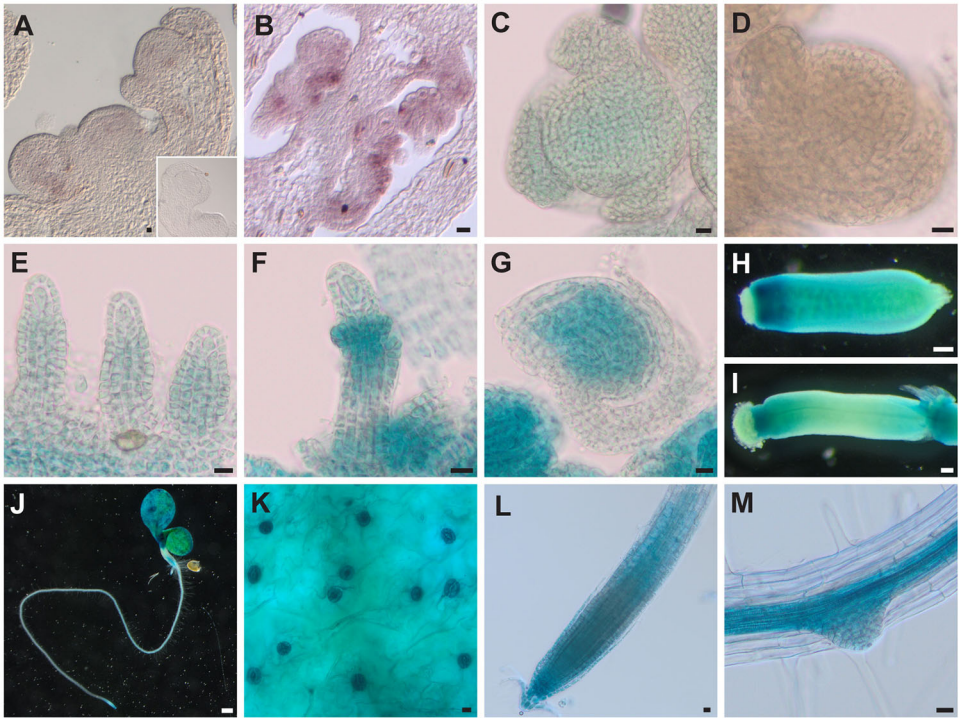

Fig. 2. Expression pattern of *ZET*. (A,B) *In situ* hybridization of sectioned stage 3 FMs (A) and stage 2-IV ovules (B) using a *ZET* antisense probe. Inset in A shows a *ZET* sense probe control. (A) Weak staining throughout tissue is observed (compare with inset). (B) Note spotty signal pattern. (C-M) Expression pattern of the pZET::GUS reporter in L*er*. (C) Whole-mount stage 3 FM. Note broad but weak signal. (D) FM from non-transgenic control plant. No signal is detectable upon equal staining treatment in comparison with C. (E-G) Ovules of stage 2-I (E), 2-III (F) and 3-VI (G). Young ovules show broad signal. Eventually, signal accumulates preferentially in the inner integument. At later stages, signal is still preferentially detectable in the inner integument. (H,I) Stage 11 and 12 carpels, respectively. Signal mainly observed in stigmatic region. (J) 5-day seedling. (K) Cotyledon epidermis. Note signal in stomata. (L) Broad signal in root meristematic region exhibited by the main root of a 5-day *pZET::GUS* seedling. (M) Signal is detectable in young lateral roots. Scale bars: 10 µm (A-G,K-M); 0.5 mm (H-J).

with that detected in *pZET::GUS* reporter lines, indicating post-transcriptional regulation of *ZET*. We could observe signal in subepidermal cells in young leaf primordia and the epidermis of cotyledons and the wall of stage 12 carpels of *pZET::TS:ZET* plants (Fig. 3A,B). Furthermore, signal was seen in the cortex of the meristematic zone of the main and lateral roots (Fig. 3C-F) and in the cortex throughout the hypocotyl. The *pUBQ::TS:ZET* reporter also showed signal in older leaves (data not shown). However, we were unable to detect a signal in FMs and ovules of both types of reporter lines indicating that the fusion protein is present at very low levels in those tissues.

When detectable, the TS:ZET signal appeared to be unequally distributed in the apoplast, particularly in cotyledon epidermis cells and the root cortex. The signal does not support a PD localization for ZET, as was observed for SUB and QKY (Vaddepalli et al., 2014). In a cross-section view, signal in the root was restricted to the six corners created by the three-way junctions that are present between an individual cortex cell and its direct neighbors (Fig. 3D). In a longitudinal view, signal appeared as short, longitudinal threads or rods with individual threads spanning one to three cells followed by short gaps (Fig. 3E,F). To confirm an apoplast localization of TS:ZET, we performed plasmolysis experiments. Upon application of 0.4 M mannitol to roots, the signal usually disappeared after 15 min and prior to observable retraction of the PM indicating a possible, treatment-induced degradation of the fusion protein. In lateral roots, however, signal could occasionally be detected after 15 to 20 min of treatment (Fig. 3G-N). In those cases, we observed a spot-like signal within the space between the retracting PMs of neighboring cells (Fig. 3I,M). Thus, signal was not detectable at the PM nor did it occupy the entire apoplastic space, as did YFP:LTPG, an apoplastic control protein (Fig. 3J,N) (Ambrose et al., 2013).

GPI anchoring is dispensable for ZET function

In the light of the apoplast localization of TS:ZET, we next tested whether the GPI anchor is essential for TS:ZET function. PredGPI, a prediction system for GPI-anchored proteins, identified amino acid S-456 as the ω site in ZET, the site of GPI anchor addition (Pierleoni et al., 2008). In the next step, we deleted the GPI anchor addition domain including the ten ω-minus amino acids (residues 448 to 480). Interestingly, the pZET::TS:ZET-ΔGPI reporter displayed weak ER-like pattern (Fig. 4A) with no obvious cell wall signal. This ER-like pattern is consistent with previous studies showing that GPI attachment is required for proper transport of GPI-anchored proteins from the ER to the cell surface, the absence of which leads to enhanced retention of these proteins in the ER (Doering and Schekman, 1996; Liu et al., 2016).

Interestingly, despite undetectable cell wall signal some *pZET::TS:ZET-ΔGPI zet-1* lines displayed wild-type morphology (Fig. 4C-F). However, removing the GPI-anchor addition domain reduced the biological activity of TS:ZET as only 19 out of 51 independent *pZET::TS:ZET-ΔGPI zet-1* transgenic lines showed complete rescue. This observation is in contrast to *pZET::TS:ZET zet-1*, as these lines exhibited 100% phenotypic rescue (44/44). We hypothesized that in the rescued *pZET::TS:ZET-ΔGPI zet-1* lines there was a very low level of ZET activity in the cell wall that was sufficient for normal ZET function. When we expressed TS:ZET-ΔGPI under the control of the *UBQ10* promoter, signal appeared in the apoplast (Fig. 4B) and all *pUBQ::TS:ZET-ΔGPI zet-1* lines exhibited a wild-type phenotype (11/11), supporting this notion. Taken together, our results demonstrate that the GPI anchor addition domain of ZET is dispensable for both its function and localization.

ZET does not affect the subcellular localization of SUB:EGFP

Next, we began to address the role of *ZET* in SUB signaling. *ZET* and *SUB* do not appear to regulate each other at the transcriptional level (Fulton et al., 2009; Vaddepalli et al., 2014). In addition, subcellular localization for TS:ZET appeared unaffected in *sub-1* mutants and the localization of functional SUB:EGFP was also not altered in *zet-1* mutants (Fig. S2). These results indicate that ZET and SUB also do not interact at the level of regulation of the subcellular distribution of the proteins.

Development (2017) 144, 2259-2269 doi:10.1242/dev.152231

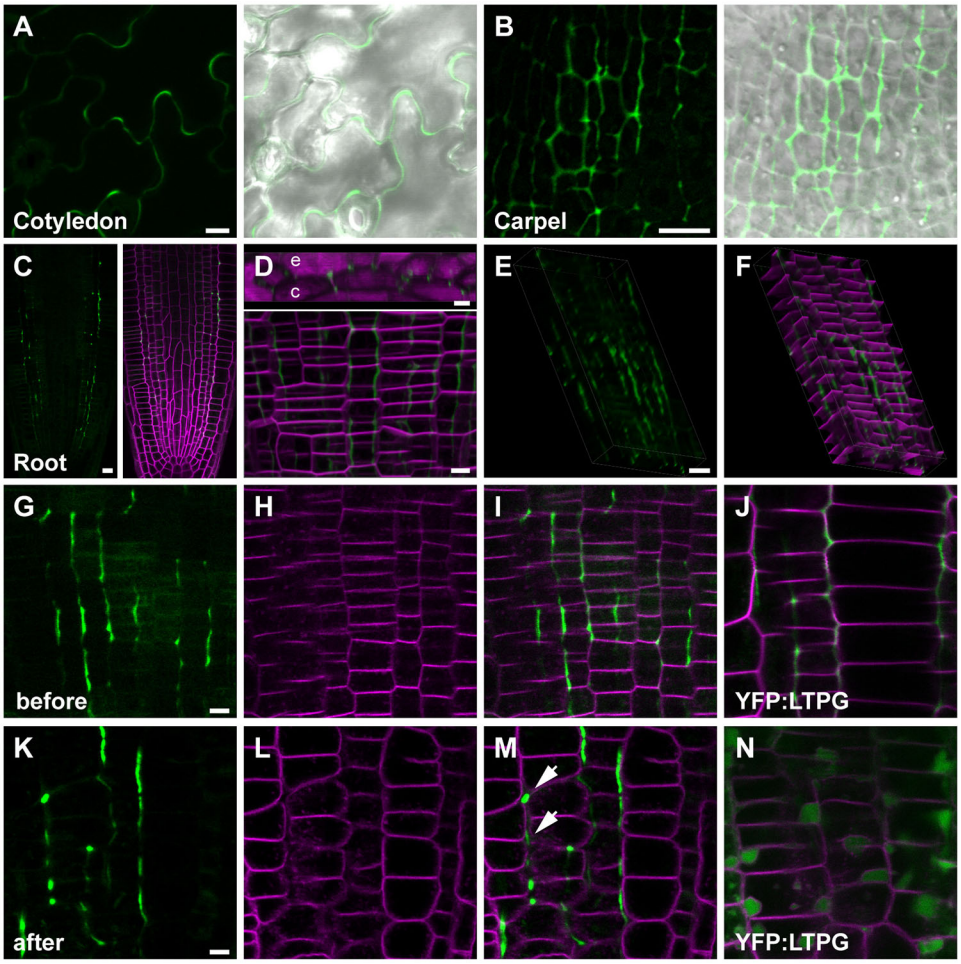

Fig. 3. Confocal micrographs of subcellular localization of reporter signal exhibited by *pZET::TS:ZET zet-1* plants. (A) Horizontal view of cotyledon epidermis. Note accumulation of signal at lobes of pavement cells. (B) Horizontal view of stage 11 carpel epidermis. Right-hand panels (A,B) include DIC channel. (C-F) Optical sections through the meristematic region of a 5-day root. Magenta signal marks the PM. Green marks TS:ZET reporter signal. (C) Mid-optical section. Note the thread-like signal around the cortex. (D-F) Different views of the same 3D-reconstructed root. (D) Top: Horizontal view showing part of the cortex (c) and epidermis (e). Note the spots at the corners around the cortex cell. Bottom: Vertical view. Note the thread-like signal pattern. (E,F) Tilted side-angle view revealing thread-like signal along one or two cells. (G-N) Plasmolysis assay in lateral root epidermis. (G-J) Signal localization before plasmolysis. (K-N) Signal localization 20 min after the addition of 0.4 M mannitol. (J,N) YFP:LTP control reporter. (M) Note focused TS:ZET signal at cell wall (arrows). (N) Control reporter shows diffuse signal throughout the apoplastic space. DIC, differential interference contrast. Scale bars: 5 µm.

ZET functions in a non-cell-autonomous fashion

Non-cell-autonomy of *SUB* and *QKY* is another important feature of *SUB* signal transduction (Kwak and Schiefelbein, 2008; Yadav et al., 2008; Vaddepalli et al., 2014). Thus, we investigated whether *ZET* functions non-cell-autonomously as well.

Young ovules show a broad *ZET* expression (Fig. 2B,E,F) and ovules of *zet* mutants generate *sub*-like abnormal integuments (Fig. 5C). During ovule development, *WUS* expression is transiently observed in the developing distal nucellus up to shortly after integument initiation when it eventually becomes undetectable

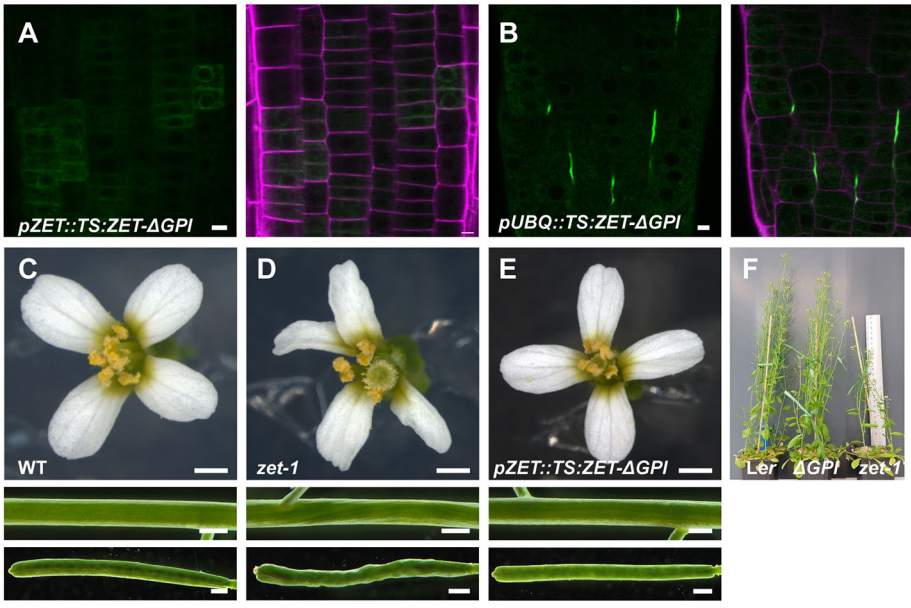

Fig. 4. GPI addition domain is dispensable. (A,B) Confocal micrographs of optical sections through the meristematic region of a 5-day *zet-1* root depicting the subcellular localization of reporter signal exhibited by the indicated mutant reporters. Right: Magenta signal marks the PM. (A) Weak endoplasmic reticulum-like pattern. (B) Normal TS:ZET signal localization. (C-E) Morphology of flowers (top), siliques (middle) and stems (bottom). Genotypes are indicated. (E) *zet-1* phenotypes are rescued by the *pZET::TS:ZET-ΔGPI* transgene. (F) Whole-plant appearance. Genotypes are indicated. ΔGPI: *pZET::TS:ZET-ΔGPI zet-1*. Scale bars: 5 µm (A,B); 0.5 mm (C-E).

Development (2017) 144, 2259-2269 doi:10.1242/dev.152231

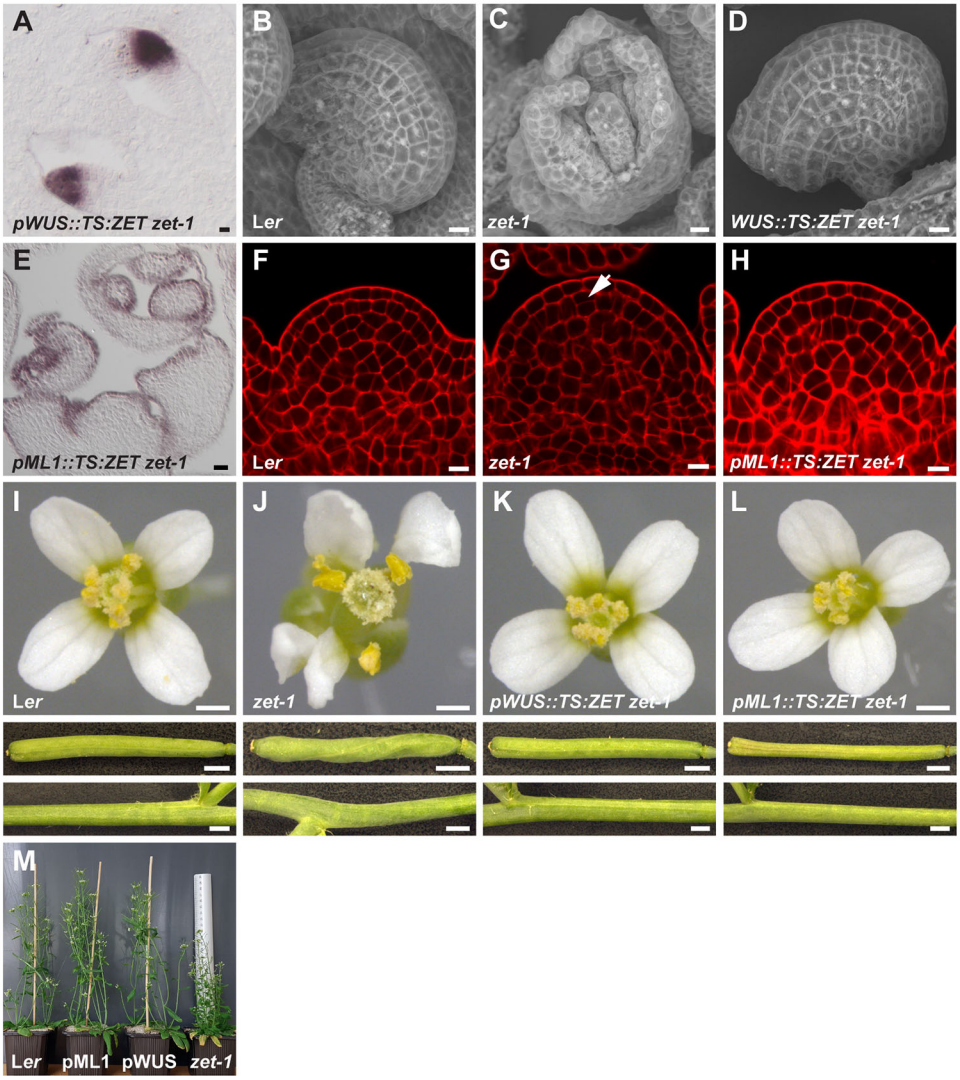

Fig. 5. Non-cell-autonomy of *ZET* function. (A) *In situ* hybridization of sectioned stage 2-II ovules of a *pWUS::TS:ZET zet-1* plant using a *GFP* antisense probe. Signal is restricted to the nucellus. (B-D) Scanning electron micrographs of late stage 3/early stage 4 ovules. (D) The *zet-1* phenotype is rescued by *pWUS::TS:ZET*. (E) *In situ* hybridization of sectioned inflorescence and young floral tissue of a *pML1::TS:ZET zet-1* plant using a *GFP* antisense probe. Note epidermis-specific signal. (F-H) Stage 3 FMs stained with pseudo-Schiff propidium iodide (mPS-PI). (G) Arrow indicates aberrant periclinal cell division in L2. (H) Note regular cell division pattern in L2. (I-L) Morphology of flowers (top), siliques (middle) and stems (bottom). Genotypes are indicated. (K,L) *zet-1* phenotypes are rescued by the respective transgenes. (M) Above-ground overall morphology of *zet-1* plants carrying *pML1::TS:ZET* (pML1) or *pWUS::TS:ZET* (pWUS) transgenes. Scale bars: 10 µm (A-H); 0.5 mm (I-L).

(Gross-Hardt et al., 2002; Bäurle and Laux, 2005). The initiating outer integument is separated from the nucellus by about five cells (Schneitz et al., 1995). To test whether restricting *TS:ZET* expression to the nucellus is sufficient for normal integument development, we generated *pWUS::TS:ZET zet-1* plants. As expected, transgene expression in the nucellus could be detected by *GFP*-based *in situ* hybridization (Fig. 5A). However, fluorescent TS:ZET reporter signal was undetectable. These results suggest that the transgene is active in the nucellus but the TS:ZET reporter protein is present at very low levels in ovule tissue, possibly due to post-transcriptional regulation. Regardless, driving *TS:ZET* expression specifically in the nucellus resulted in near-regular integument development as ovules of *pWUS::TS:ZET zet-1* plants developed normally (Fig. 5B-D). This result indicates that *ZET* can influence the development of cells, several cells distant from where its mRNA is produced.

pWUS::TS:ZET zet-1 plants also exhibited normal floral morphology and wild-type plant stature (Fig. 5I-K,M) indicating that restricting expression of *TS:ZET* to a few cells in internal layers of shoot apical and floral meristems (Mayer et al., 1998) is sufficient to rescue stem and flower development in *zet-1* mutants.

ZET is broadly expressed in FMs (Fig. 2A,C) and *zet* mutants display altered floral morphology and cell division planes in cells of the L2 layer (Fig. 5F,G; Table 1) (Fulton et al., 2009). By contrast, *ML1* is specifically expressed in the L1 of shoot and FMs and in the epidermis of young floral organs (Lu et al., 1996; Sessions et al., 1999). Moreover, expression of a pML1::NLS:GFP reporter was restricted to the epidermis of FMs in wild-type or *zet-1* plants indicating that *ML1* promoter activity is not influenced by *ZET* (Fig. S3A,B). We investigated whether restricting the expression of *TS:ZET* to the L1 cells of FMs can rescue the L2 division plane defects of *zet-1* mutants. We were unable to detect TS:ZET signal in the shoot apex and floral tissues of *pML1::TS:ZET zet-1* lines. However, *in situ* hybridization with a *GFP* probe revealed transgene expression in the L1 layer as expected (Fig. 5E). These results suggest that the transgene is active in the epidermis but the TS:ZET reporter protein is present at very low levels in floral tissue.

Table 1. Number of periclinal cell divisions in the L2 layer of stage 3 floral meristems

Genotype	NPCD*	% (NPCD/NFM)	NFM‡
Ler	3	6.7	45
zet-1	15	35.7	42
pML1::TS:ZET zet-1	2	3.4	58

*Number of periclinal cell divisions observed.
‡Number of floral meristems observed.

Development (2017) 144, 2259-2269 doi:10.1242/dev.152231

Interestingly, we observed wild-type numbers of periclinal L2 division planes in *pML1::TS:ZET zet-1* FMs (Fig. 5H; Table 1) indicating that *TS:ZET* expression in L1 cells influences the neighboring mutant L2 cells. In addition, *pML1::TS:ZET zet-1* plants also exhibited normal floral and stem morphology and showed wild-type plant height and stature (Fig. 5I,J,L,M).

TS:ZET reporter signal, however, was detectable in lateral roots of *pML1::TS:ZET zet-1* plants. Interestingly, although the *ML1* promoter is active in the root epidermis (Sessions et al., 1999) (Fig. 6A,B) (Fig. S3G) and its activity is independent of *ZET* in the root as well (Fig. 6B), TS:ZET signal was also detectable in the apoplast between cortex and endodermis cells in wild type or in *sub-1* (Fig. 6C-E). This observation indicates that the TS:ZET fusion protein can spread to neighboring cells in lateral roots in a *SUB*-independent fashion.

Taken together, our data suggest that *ZET* acts non-cell-autonomously across several cells.

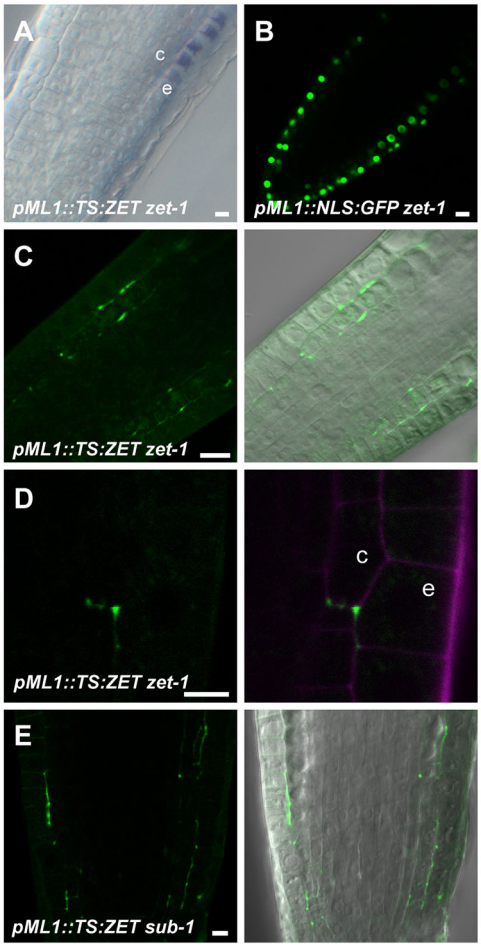

Fig. 6. TS:ZET spreads locally in lateral roots. Genotypes are indicated. (A) Whole-mount *in situ* hybridization of a lateral root using a *GFP* antisense probe. Signal is restricted to epidermis. (B) Control using a nuclear-localized pML1::NLS:GFP reporter. Signal can be seen in the root cap and the epidermis. (C) Confocal micrograph depicting a mid-optical section through a lateral root. Note TS:ZET signal between the cortex and endodermis. Right-hand panel includes DIC channel. (D) Confocal micrograph highlighting an epidermis-cortex region of a different lateral root compared with that shown in C. Note signal distribution along the entire basal side of indicated cortex cell. (E) Note the TS:ZET signal at cortex/endodermis interface in *sub-1* (compare with C). Right-hand panel includes DIC channel. c, cortex; DIC, differential interference contrast; e, epidermis. Scale bars: 10 µm.

ZET represents an atypical BG

To assess further the role of ZET in SUB signaling we focused on its biochemical function. Sequence analysis indicated that ZET carries putative hydrolytic GH17 and CBM43 domains, which are typically involved in hydrolyzing and binding β-1,3 glucans, respectively (Fig. 7A). Its GH17 domain features the typical two glutamic acids (E265, E326) that were biochemically shown to be essential for catalytic activity of the barley BG GII (Chen et al., 1993). The two glutamic acids are also highly conserved among BG family members (Doxey et al., 2007; Gaudioso-Pedraza and Benitez-Alfonso, 2014). Moreover, the CBM43 domain of ZET contains all the conserved cysteines [C367-x(19)-C-x(4)-C-x(8)-C401-x(26)-C-x(17)-C] that are the hallmarks of the *Arabidopsis* CBM43 domain consensus (Doxey et al., 2007; Simpson et al., 2009). Thus, ZET is predicted to be a typical callose-degrading BG.

To assay biochemically whether ZET can bind callose, we expressed in *Escherichia coli* a recombinant near full-length protein that included the GH17 and CBM43 domains but lacked the N-terminal signal peptide and the C-terminal hydrophobic residues required for the connection to a GPI moiety. We fused a thioredoxin:6xHis tag to the N terminus of ZET (thioredoxin:ZET) as ZET function is unaffected by tags at this site *in planta*.

To test whether thioredoxin:ZET can bind to callose, we performed nondenaturing gel retardation assays. In gels that included laminarin, a long-chain β-1,3 glucan also containing β-1,6 branches, recombinant CBM43-domain control protein thioredoxin:PDCB1 exhibited reduced migration relative to bovine serum albumin and to thioredoxin:PDCB1 in the absence of laminarin (Fig. 7B). This result indicates binding of the fusion protein to laminarin as expected (Simpson et al., 2009). By contrast, thioredoxin:ZET showed an identical migration pattern in the presence or absence of laminarin (Fig. 7B). This result suggests that thioredoxin:ZET is unable to bind to laminarin *in vitro*.

The biochemical experiment mentioned above supports the notion that ZET might not degrade callose. However, it could be misleading owing to potential technical issues. For example, the presence of β-1,6 branches in laminarin could interfere with TS:ZET binding or the recombinant fusion protein could be misfolded or lack post-translational modifications (Fig. S1). Thus, we set out to relate ZET function to callose degradation *in planta*. To this end, we performed several *in vivo* assays. First, we assessed wound-induced callose accumulation in leaves (Fig. 7C-F). Upon wounding, callose accumulation was strongly induced in wild-type leaves. However, wound-induced callose accumulation did not noticeably change in comparison with wild type in leaves of *zet-1* or two different transgenic *pUBQ::TS:ZET* lines (Fig. 7D,E). By contrast, callose accumulation was noticeably reduced in leaves overexpressing plasmodesmal-localized BG1 (PdBG1) (Fig. 7F), confirming previous results (Benitez-Alfonso et al., 2013). We also tested intercellular GFP movement as regulated callose turnover at PD controls movement of molecules through PD (Zavaliev et al., 2011; De Storme and Geelen, 2014). However, diffusion of GFP through PD appeared to be unaffected in plants with altered *ZET* activity (Fig. S3). Finally, we did not observe *ZET*-dependent effects when examining bacterial flagellin-induced callose deposits in cotyledons incubated with the elicitor flg22 (Felix et al., 1999) or when analyzing phototropism in seedlings, a process known to depend on PD-associated callose accumulation (Han et al., 2014) (Fig. S4). Taken together, these genetic results indicate that *ZET* does not contribute to callose degradation *in vivo*.

To gain further insight into this issue, we performed genetic complementation experiments. Using site-directed mutagenesis we

Development (2017) 144, 2259-2269 doi:10.1242/dev.152231

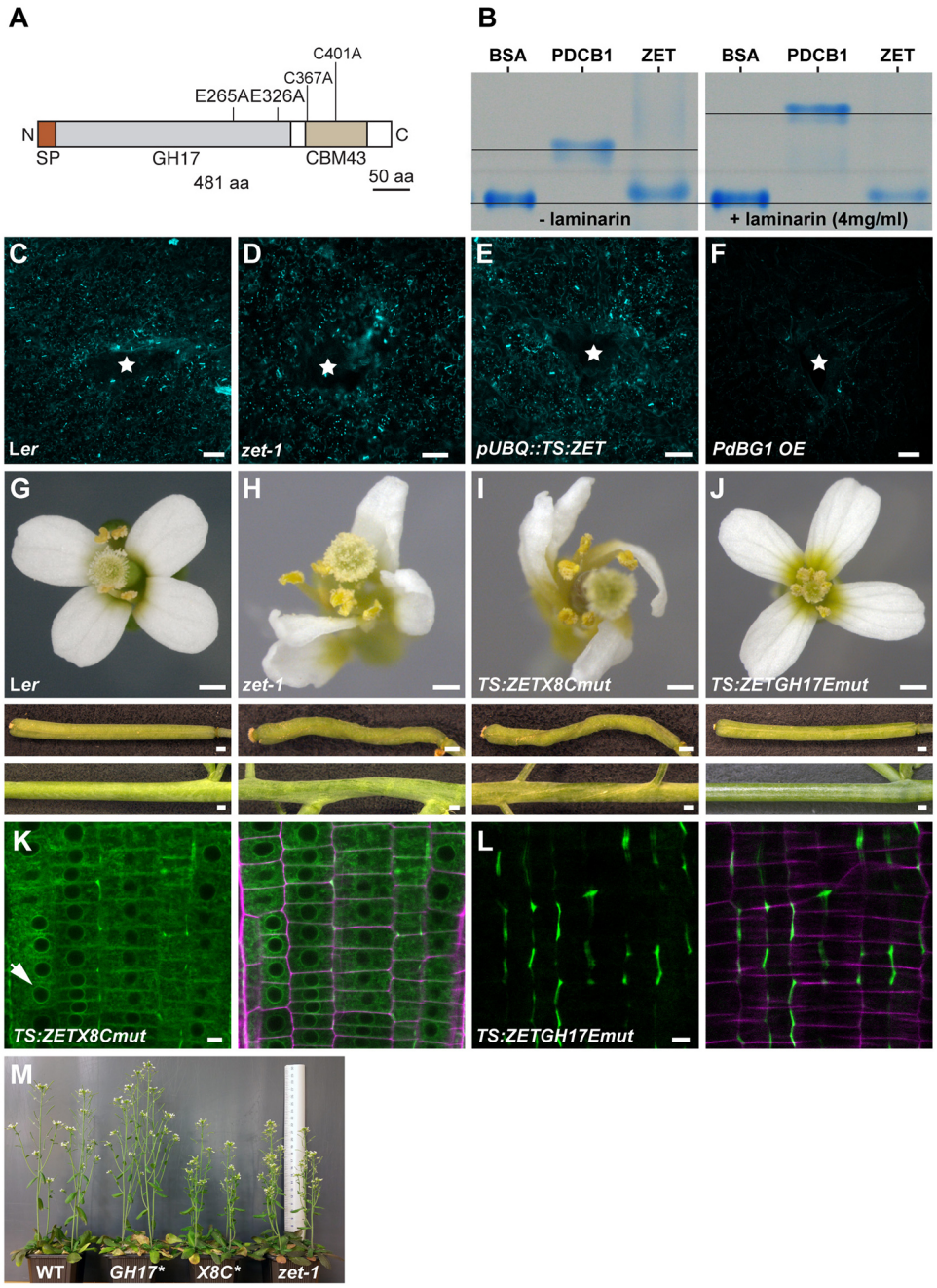

Fig. 7. ZET is an atypical BG.
(A) Schematic highlighting the altered ZET residues. (B) Coomassie Blue gel depicting typical result of gel retardation assays using thioredoxin:PDCB1 and thioredoxin:ZET recombinant proteins. Migration of thioredoxin:ZET is independent of laminarin. (C-F). Aniline Blue-based wounding assays. Stars mark the wounded area of the leaf. The *PdBG1* overexpression line (control) shows reduced Aniline Blue signal. (G-J) Morphology of flowers (top), siliques (middle) and stems (bottom). Genotypes are indicated. (J) *zet-1* phenotypes are rescued by the *pUBQ::TS:ZETGH17Emut* transgene. (K,L). Confocal micrographs of optical sections through the meristematic region of a 5-day *zet-1* root depicting the subcellular localization of reporter signal exhibited by the indicated mutant reporters. Right-hand panel includes propidium iodide staining in magenta. (K) An ER-like pattern is indicated by the arrow. (L) Normal TS:ZET signal localization. (M) Whole-plant appearance. Genotypes are indicated. GH17*: *pUBQ::TS:ZETGH17Emut zet-1*; X8C*: *pUBQ::TS:ZETX8Cmut zet-1*. Scale bars: 10 µm (C-F); 0.5 mm (G-J); 5 µm (K,L).

altered two conserved cysteines to alanine (C367A, C401A) in the CBM43 domain generating the mutant reporter gene *TS:ZETCmut*. *pUBQ::TS:ZETCmut zet-1* plants showed a mutant phenotype indicating that the mutant reporter gene was nonfunctional (Fig. 7I) (46 T1 lines/46 total). Confocal microscopy revealed an essentially ER-like subcellular distribution of the reporter signal in roots with only rare occurrences of signal in the apoplast (Fig. 7K). These results suggest that C367 and C401 are required for correct subcellular localization and/or function of ZET.

Next, we altered both conserved glutamic acids of the GH17 domain of ZET to alanine (E265A, E326A) generating the mutant reporter *TS:ZETGH17Emut* carrying both mutations. The two glutamic acids were biochemically shown to be essential for catalytic activity of BGs (Chen et al., 1993). Surprisingly, *pUBQ::TS:ZETGH17Emut zet-1* plants exhibited wild-type morphology (Fig. 7J) (32 T1 lines/32 total). Moreover, subcellular distribution of TS:ZETGH17Emut reporter signal in roots appeared normal (Fig. 7L). These results indicate that the mutant reporter was biologically active.

Taken together, the results suggest that ZET cannot bind to laminarin *in vitro*, does not degrade callose *in planta*, and that the two conserved glutamic acids of its GH17 domain are not required for its function *in vivo*. Thus, ZET could be a catalytically inactive BG-like protein.

ZET, *SUB* and *QKY* affect cell wall structure

The observed cell wall localization of the TS:ZET reporter raised the question whether ZET affects cell wall composition. To address this question, Fourier-transformed infrared-spectroscopy (FTIR) was performed on cell wall preparations obtained from stage 1-13 flowers of *zet-2*. This study was also extended to *sub-1* and *qky-8* mutants (Fig. 8). Interestingly, the spectra of all three mutants

Development (2017) 144, 2259-2269 doi:10.1242/dev.152231

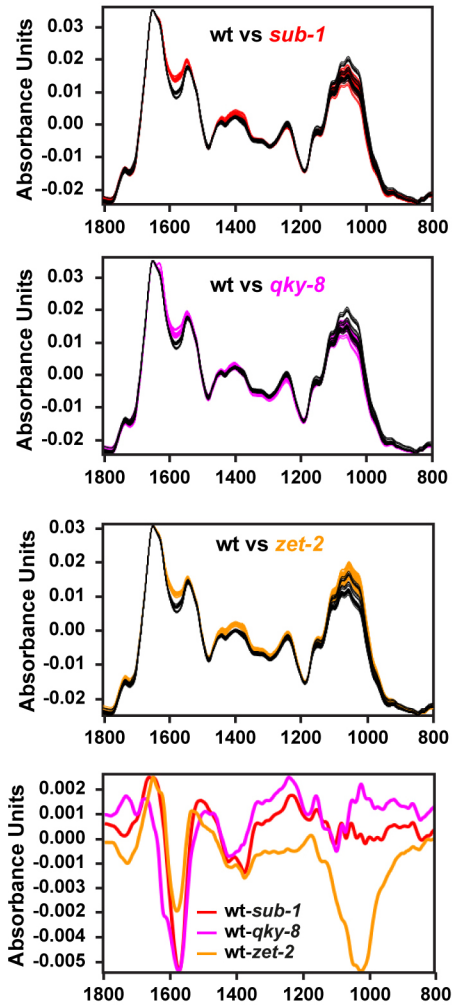

Fig. 8. SUB signaling affects cell wall chemistry. FTIR analysis. Each of the three top panels shows an overlay of the spectra of three biological replicates, with ten technical replicates each, for the indicated genotype (total of 30 spectra each). The bottom panel depicts the difference spectra obtained by digital subtraction from wild type of the average spectra of the indicated genotypes.

showed notable and near-identical deviations from wild type in the range of 1350 to 1700 cm^{-1}. The *zet-2* spectrum showed an additional and unique difference around 1000 to 1100 cm^{-1}. Thus, our data reveal that *ZET*, *SUB* and *QKY* directly or indirectly influence cell wall composition in an overlapping fashion with *ZET* having an additional effect on the cell wall as well.

DISCUSSION

Here, we present a molecular and functional characterization of *ZET*. The data suggest that ZET is an atypical BG and an extracellular protein. Moreover, they indicate that *ZET* and *SUB* are involved in the control of cell wall organization.

As a putative BG with a role in tissue morphogenesis, ZET joins a remarkably small group of known developmentally important BGs. Historically, BGs were mainly studied with respect to their role as pathogenesis-related (PR) proteins in the context of stress responses (Leubner-Metzger and Meins, 1999). For example, the *Arabidopsis* BG AtBG_ppap localizes to PD, affects callose accumulation at PD upon wounding and regulates PD flux (Levy et al., 2007; Zavaliev et al., 2013). More recently, however, it became clear that the two PD-localized BGs PdBG1 and PdBG2 play a prominent role in early lateral root formation through the regulation of PD conductivity by modulating callose accumulation at PD (Benitez-Alfonso et al., 2013). Moreover, PD-localized BG are thought to be involved in opening signaling conduits required for the release of apical bud dormancy in *Populus* (Rinne et al., 2011).

Interestingly, ZET differs from the above-mentioned BGs as our data do not support a PD localization of ZET. Rather, they suggest that ZET is localized to the cell wall. GPI-anchored proteins are expected to localize to the outer leaflet of the PM and ZET was identified in two proteomic analyses of GPI-anchored membrane proteins performed using cell suspension cultures (Elortza et al., 2003, 2006). However, we did not detect a PM signal for TS:ZET. In addition, PM-anchored TS:ZET does not appear to be biologically essential as we found that the GPI anchor addition domain is dispensable for the biological activity of TS:ZET. An analogous observation was made for the GPI-anchored protein LORELEI (LRE) (Liu et al., 2016). Interestingly, for many fungal GPI-anchored proteins the final destination is not the PM. An additional processing of the GPI anchor targets those proteins directly to the cell wall (Orlean and Menon, 2007). Based on our existing data, it is possible that ZET undergoes a similar post-translational processing step before it is targeted to the extracellular matrix. In that case, this additional processing event of GPI proteins will be a characteristic of fungi and plants as there is no counterpart in mammals. Severing of the GPI moiety and subsequent localization of the processed protein to the extracellular matrix has been observed in plants (Oxley and Bacic, 1999; Schultz et al., 2000) but so far cell wall localization is arguably best documented for the GPI-anchored protein COBRA (COB) from *Arabidopsis* and Brittle Culm1, a COBRA-like protein in rice (Roudier et al., 2005; Liu et al., 2013).

The finding that TS:ZET localizes to the cell wall is in line with a recent phylogenetic study of the GH17 family suggesting that PD-localized proteins belong to the clade alpha whereas members of clade beta, which includes ZET, were suggested to be localized to apoplast (Gaudioso-Pedraza and Benitez-Alfonso, 2014). Apart from its apoplastic localization, our FTIR analysis implicates a role for ZET in cell wall structure. Thus, for future studies it would be interesting to investigate whether all the other members of beta clade also show similarities in localization and a role in cell wall biology.

We observed TS:ZET signal in the apoplast between the cortex and endodermis cells of *pML1::TS:ZET zet-1* lateral roots. This finding indicates that ZET is able to spread locally through the apoplast from its site of synthesis in the epidermis to the neighboring cortex/endodermis interface. The notion of ZET as a mobile extracellular protein is also supported by its presence in the culture filtrate proteome of *Arabidopsis* suspension cells (Tran and Plaxton, 2008).

The apoplastic localization of TS:ZET and the cell wall defects in *zet* mutants support a role for ZET in controlling the composition of the cell wall. Sequence analysis suggested ZET to be a bona fide BG predicted to degrade the cell wall polymer callose. Recombinant ZET, however, did not bind to laminarin in an *in vitro* binding assay. Moreover, loss- or gain-of-function of ZET did not lead to detectable effects on callose degradation in several *in planta* assays. Finally, mutating the two conserved glutamate residues of the GH17 domain of ZET failed to impair its ability to complement the *zet* phenotype. Collectively, these findings suggest that ZET is not involved in callose turnover and might encode a catalytically inactive or atypical BG. We are unaware of a similar report in the literature. Still, non-catalytic enzymes involved in carbohydrate metabolism have been described before and have been implied to play regulatory roles

Development (2017) 144, 2259-2269 doi:10.1242/dev.152231

in the respective pathways. For example, tobacco NIN88 is a catalytically defective cell wall invertase that was proposed to regulate sucrose cleavage by controlling the interaction between a regular cell wall invertase and the cell wall (Le Roy et al., 2013). Another example is *Arabidopsis* β-AMYLASE 4 (BAM4) a non-catalytic enzyme regulating starch breakdown upstream of three enzymatically active β-amylases in a still unresolved fashion (Fulton et al., 2008). Unlike NIN88 or BAM4, which feature prominent structural alterations, the primary sequence of ZET does not provide an obvious explanation for its apparent lack of enzymatic activity behavior. Thus, the molecular basis for the atypical activity of ZET remains to be explored. Regardless, in analogy to the above-mentioned examples we propose that ZET does not exert an enzymatic function but rather plays a regulatory role in the control of cell wall biology and tissue morphogenesis.

Apart from the functional overlap between *SUB* and *QKY* in controlling tissue morphogenesis and root hair patterning, our FTIR data reveal that absence of *SUB* or *QKY* function also results in very similar cell wall defects in flowers, thus connecting SUB signaling to the control of cell wall composition. The data further show correspondence but also distinction between the floral cell wall defects of *zet* or *sub* and *qky*, respectively, indicating that *ZET* plays an additional role in cell wall organization.

How does ZET relate to the SUB signaling mechanism? Our evidence suggests that ZET functions in a non-cell-autonomous fashion and is able to spread locally through the apoplast. ZET is unlikely to be a component of the SMS signal as *SUB* does not affect TS:ZET localization. This indicates that there is a difference between the non-cell-autonomy of *ZET* and *SUB*. Alternatively, a cell wall mechanism that depends on ZET and SUB could establish a basis for SMS function that, for example, would facilitate the passage of SMS through PD or via the apoplast. We currently favor a scenario in which ZET and SUB act in separate pathways that converge upstream of the control of cell wall composition. This notion is in accordance with the similarity of the *sub* and *zet* phenotypes, the exaggerated phenotype of *zet sub* double mutants, and the absence of cross-regulation between the two genes at the level of transcription (Fulton et al., 2009) or protein localization. In addition, the overexpression phenotype of *SUB* does not depend on *ZET*, and ZET fails to interact with the extracellular domain of SUB in yeast two-hybrid assays (Fig. S5). These two findings also render it unlikely that ZET functions on the ligand side of SUB signaling or that ZET acts as an essential co-receptor for SUB as it was proposed for the GPI-anchored protein LLG1 and the RLK FER (Li et al., 2015). It will be very interesting to investigate in more detail how an atypical RLK and an atypical BG integrate cell wall biology, PD-dependent signaling, and tissue morphogenesis.

MATERIALS AND METHODS

Plant work, plant genetics and plant transformation

Arabidopsis thaliana (L.) Heynh. var. Columbia (Col-0) and var. Landsberg (*erecta* mutant) (L*er*) were used as wild-type strains. Plants were grown as described previously (Fulton et al., 2009). The *zet-1*, *sub-1* and *qky-8* mutants (all in L*er*) were described previously (Chevalier et al., 2005; Fulton et al., 2009). The Ds-transposon-induced *zet-2* mutant (L*er*) was obtained from the GeneTrap collection at Cold Spring Harbor (ET13436) (Sundaresan et al., 1995). Wild-type and *zet-1* mutant plants were transformed with different constructs using *Agrobacterium* strain GV3101/pMP90 (Koncz and Schell, 1986) and the floral dip method (Clough and Bent, 1998). Transgenic T1 plants were selected on kanamycin (50 µg/ml), hygromycin (20 µg/ml) or glufosinate (Basta) (10 µg/ml) plates and transferred to soil for further inspection.

Recombinant DNA work

For DNA and RNA work, standard molecular biology techniques were used. PCR fragments used for cloning were obtained using Phusion high-fidelity DNA polymerase (New England Biolabs) or TaKaRa PrimeSTAR HS DNA polymerase (Lonza). PCR fragments were subcloned into pLitmus 28i (NEB) or pENTR 1A (Life Technologies). All PCR-based constructs were sequenced. The plasmid pEGAD (Cutler et al., 2000) and the Gateway-based (Invitrogen) destination vector pMDC32 (Curtis and Grossniklaus, 2003) were used as binary vectors. Primer sequences used in this work are listed in Table S2.

Reporter constructs

For plasmid pZET::GUS pEGAD, 1.4 kb of promoter sequence spanning genomic DNA up to the 3′ end of the next gene was amplified from L*er* genomic DNA using primers Kpn1_pZET_F/pZET_Asc1_R and cloned into GUS pEGAD. T-Sapphire and ZET genomic sequences were fused by overlapping PCR using primers TS_F/TS_R and pZET_F/pZET_R cloned into pEGAD pZET::GUS replacing GUS to obtain pZET::TS:ZET. For pZET::TS:ZET ΔGPI construct, a stop codon was introduced before the GPI addition domain using primers ZET F448*_F/ ZET F448*_R. Cloning of the pML1 and pWUS promoters was described previously (Vaddepalli et al., 2014). pML1::TS:ZET, pWUS::TS:ZET, pUBQ::TS:ZET, pUBQ::TS:ZETCmut, pUBQ::TS:ZETGH17Emut and pUBQ::TS:ZET ΔGPI were obtained by Gateway cloning and *in vitro* mutagenesis. All constructs were verified by sequencing. For details of map-based cloning of *ZET*, see supplementary Materials and Methods.

Generation, expression and purification of recombinant proteins

ZET and PDCB1 coding sequences lacking the N- and C-terminal signals were amplified from stage 1-12 floral cDNA (L*er*) with primers ZETGH_EcoRI_F/ZET_XhoI_R and PDCB1_EcoRI_F/PDCB1_Xho1_R, respectively, and cloned into p32a (Invitrogen). The clones were expressed in the *E. coli* strain BL21 (DE3) pLysS. Expression from the pET32a vector leads to proteins fused to an N-terminal thioredoxin protein and a 6x histidine tag. For protein expression and purification, bacterial cultures were grown to OD 0.6-0.8 at 30°C. Then, the bacteria were induced with 0.5 mM isopropyl-beta-thio galactopyranoside and grown overnight at 21°C. Subsequently, the recombinant proteins were purified from the overnight-grown bacteria by immobilized metal ion affinity chromatography under native conditions using the Protino Ni-TED 2000 Kit (Macherey-Nagel) according to the manufacturer's protocol. The resulting proteins were concentrated using Amicon Ultra-4 30 K (30,000 NMWL) centrifugal filter devices (Merck Millipore).

In vitro laminarin binding assays

Thioredoxin-ZET binding to Laminarin was assessed using gel retardation assay as described by Simpson et al. (2009). Briefly, 12% non-denaturing PAGE gels were prepared containing 4 mg/ml of the polysaccharide laminarin in the resolving gel. The purified thioredoxin-ZET and thioredoxin-PDCB fusion proteins were loaded onto the gels after mixing with 2× sample buffer and electrophoresed at 120 V for 3 h at room temperature. Coomassie Brilliant Blue staining was carried out to visualize proteins.

Western blot analysis

TissueLyser II (Qiagen) was used to lyse 50 mg of 6-day-old wild-type or transgenic seedlings. Samples mixed with 2× Laemmli buffer and heated at 50°C for 10 min. Extracts were centrifuged at 13,000 rpm (15,700 ***g***) for 5 min and loaded onto SDS-PAGE gels. SDS-PAGE and immunoblotting using polyclonal anti-rabbit GFP (Invitrogen, A-11122; 1:5000) and goat anti-rabbit HRP (Invitrogen, 65-6120; 1:5000) antibodies were performed according to standard protocols.

Fourier-transformed infrared-spectroscopy (FTIR)

Inflorescence tips of 6-week-old *Arabidopsis* plants were pre-cleaned by treating with 70% ethanol. After overnight incubation in methanol:chloroform (1:1; v:v), the tissue was washed twice with acetone and then homogenized by ball milling. Homogenized biomass (25 µl) was placed on a zinc selenide

Development (2017) 144, 2259-2269 doi:10.1242/dev.152231

sample carrier and air-dried at room temperature. FTIR spectra were recorded in transmission in the spectral range between 4000 and 500 cm^{-1} using a Tensor 27 spectrometer coupled to the HTS-XT device for high-throughput measurements (Bruker Optics) and the following parameter settings: resolution of 6 cm^{-1}, Blackman-Harris 3-Term apodization and zerofilling of 4. For each spectrum, 32 scans were recorded and averaged. Data processing was performed using OPUS 7.2 software (Bruker Optics). The first derivative of spectra was calculated and smoothed with a 9-point Savitzky-Golay filter to overcome difficulties arising from baseline shifts and to improve the resolution of complex bands. Subsequently, vector normalization was performed over the whole spectral range to compensate for variations in biomass between different samples.

Microscopy, *in situ* hybridization and imaging

To assay flg22-induced callose deposits in cotyledons seeds were surface-sterilized and grown in 24-well plates in liquid MS-medium as described by Ranf et al. (2012). Eight- to ten-day-old seedlings were exposed to 1 µm flg22. After 24 h incubation under light, seedlings were de-stained in 95% ethanol for 16 h. Seedlings were once washed in 80% ethanol, twice in 50% ethanol and twice in 100% ethanol. Subsequently, seedlings were incubated in 0.1 M Na_2HPO_4 (pH 9) for 1 h followed by Aniline Blue staining. Confocal laser scanning microscopy using staining with Aniline Blue, pseudo-Schiff propidium iodide (mPS-PI) or detection of EGFP and FM4-64 was performed primarily as described (Vaddepalli et al., 2014). T-Sapphire was excited with a 405 nm laser and the emission was detected at 505 to 540 nm. Three-dimensional reconstructions were produced with MorphographX software (Barbier de Reuille et al., 2015). Histochemical localization of β-glucuronidase (GUS) activity in whole-mount tissue and scanning electron microscopy was performed as reported previously (Schneitz et al., 1997; Sieburth and Meyerowitz, 1997). *In situ* hybridization on sections with digoxigenin-labeled probes has been described previously (Sieber et al., 2004). *ZET* antisense probe (965 bp) was obtained by PCR using primers ZETas_Insitu_F/ZETas_InsituM_R (Table S2). The sense control was obtained by using primer pair ZETsense_Insitu_F/ ZETsense_InsituM_R. Slides were viewed with an Olympus BX61 upright microscope using DIC optics. Whole-mount *in situ* hybridization using a *GFP* antisense probe was essentially performed as described (Hejatko et al., 2006). Images were adjusted for color and contrast using Adobe Photoshop CS5 software.

Acknowledgements

We acknowledge Sophie Brameyer for help with the analysis of the *ZET* expression pattern, Maxi Oelschner for expert technical assistance, and Mareike Wenning for help with the FTIR analysis. We thank Geoffrey Wasteneys for the YFP:LTPG plasmid, Xuelin Wu and Detlef Weigel for the pML1::2×GFP and pML1::NLS:GFP plasmids, Christine Faulkner and Andrew Maule for the thioredoxin:PDCB1 construct, Yoselin Benitez-Alfonso for *PDBG1 OE* seeds, and Ruth Stadler for the pSUC2::GFP and pSUC2::tmGFP9 plasmids. We also thank Ulrich Z. Hammes, Mathias Schuetz, Dolf Weijers and Sebastian Wolf for critical reading of the manuscript.

Competing interests

The authors declare no competing or financial interests.

Author contributions

Conceptualization: P.V., L.F., S.R., K.S.; Formal analysis: P.V., S.R., K.S.; Investigation: P.V., L.F., J.W., K.W., M.S.; Writing - original draft: K.S.; Writing - review & editing: P.V., K.S.; Visualization: P.V., K.S.; Supervision: K.S.; Project administration: K.S.; Funding acquisition: K.S.

Funding

This work was funded by grants from the Deutsche Forschungsgemeinschaft (German Research Council; DFG) [SFB924 (TP B10) to S.R.; SCHN 723/6-1 and SFB924 (TP A2) to K.S.].

Supplementary information

Supplementary information available online at
http://dev.biologists.org/lookup/doi/10.1242/dev.152231.supplemental

References

Ambrose, C., DeBono, A. and Wasteneys, G. (2013). Cell geometry guides the dynamic targeting of apoplastic GPI-linked lipid transfer protein to cell wall elements and cell borders in Arabidopsis thaliana. *PLoS One* **8**, e81215.

Barbier de Reuille, P., Routier-Kierzkowska, A. L., Kierzkowski, D., Bassel, G. W., Schüpbach, T., Tauriello, G., Bajpai, N., Strauss, S., Weber, A., Kiss, A. et al. (2015). MorphoGraphX: a platform for quantifying morphogenesis in 4D. *Elife* **4**, 05864.

Barral, P., Suárez, C., Batanero, E., Alfonso, C., Alché Jde, D., Rodríguez-García, M. I., Villalba, M., Rivas, G. and Rodríguez, R. (2005). An olive pollen protein with allergenic activity, Ole e 10, defines a novel family of carbohydrate-binding modules and is potentially implicated in pollen germination. *Biochem. J.* **390**, 77-84.

Bäurle, I. and Laux, T. (2005). Regulation of *WUSCHEL* transcription in the stem cell niche of the Arabidopsis shoot meristem. *Plant Cell* **17**, 2271-2280.

Benitez-Alfonso, Y., Faulkner, C., Pendle, A., Miyashima, S., Helariutta, Y. and Maule, A. (2013). Symplastic intercellular connectivity regulates lateral root patterning. *Dev. Cell* **26**, 136-147.

Chen, L., Fincher, G. B. and Høj, P. B. (1993). Evolution of polysaccharide hydrolase substrate specificity. Catalytic amino acids are conserved in barley 1,3-1,4- and 1,3-beta-glucanases. *J. Biol. Chem.* **268**, 13318-13326.

Chevalier, D., Batoux, M., Fulton, L., Pfister, K., Yadav, R. K., Schellenberg, M. and Schneitz, K. (2005). *STRUBBELIG* defines a receptor kinase-mediated signaling pathway regulating organ development in *Arabidopsis*. *Proc. Natl. Acad. Sci. USA* **102**, 9074-9079.

Clough, S. J. and Bent, A. F. (1998). Floral dip: a simplified method for *Agrobacterium*-mediated transformation of *Arabidopsis thaliana*. *Plant J.* **16**, 735-743.

Curtis, M. D. and Grossniklaus, U. (2003). A gateway cloning vector set for high-throughput functional analysis of genes in planta. *Plant Physiol.* **133**, 462-469.

Cutler, S. R., Ehrhardt, D. W., Griffitts, J. S. and Somerville, C. R. (2000). Random GFP::cDNA fusions enable visualization of subcellular structures in cells of *Arabidopsis* at a high frequency. *Proc. Natl. Acad. Sci. USA* **97**, 3718-3723.

De Storme, N. and Geelen, D. (2014). Callose homeostasis at plasmodesmata: molecular regulators and developmental relevance. *Front. Plant Sci.* **5**, 138.

Doering, T. L. and Schekman, R. (1996). GPI anchor attachment is required for Gas1p transport from the endoplasmic reticulum in COP II vesicles. *EMBO J.* **15**, 182-191.

Doxey, A. C., Yaish, M. W., Moffatt, B. A., Griffith, M. and McConkey, B. J. (2007). Functional divergence in the Arabidopsis beta-1,3-glucanase gene family inferred by phylogenetic reconstruction of expression states. *Mol. Biol. Evol.* **24**, 1045-1055.

Elortza, F., Nuhse, T. S., Foster, L. J., Stensballe, A., Peck, S. C. and Jensen, O. N. (2003). Proteomic analysis of glycosylphosphatidylinositol-anchored membrane proteins. *Mol. Cell. Proteomics* **2**, 1261-1270.

Elortza, F., Mohammed, S., Bunkenborg, J., Foster, L. J., Nühse, T. S., Brodbeck, U., Peck, S. C. and Jensen, O. N. (2006). Modification-specific proteomics of plasma membrane proteins: identification and characterization of glycosylphosphatidylinositol-anchored proteins released upon phospholipase D treatment. *J. Proteome Res.* **5**, 935-943.

Felix, G., Duran, J. D., Volko, S. and Boller, T. (1999). Plants have a sensitive perception system for the most conserved domain of bacterial flagellin. *Plant J.* **18**, 265-276.

Fujita, M. and Kinoshita, T. (2012). GPI-anchor remodeling: potential functions of GPI-anchors in intracellular trafficking and membrane dynamics. *Biochim. Biophys. Acta* **1821**, 1050-1058.

Fulton, D. C., Stettler, M., Mettler, T., Vaughan, C. K., Li, J., Francisco, P., Gil, M., Reinhold, H., Eicke, S., Messerli, G. et al. (2008). Beta-AMYLASE4, a noncatalytic protein required for starch breakdown, acts upstream of three active beta-amylases in *Arabidopsis* chloroplasts. *Plant Cell* **20**, 1040-1058.

Fulton, L., Batoux, M., Vaddepalli, P., Yadav, R. K., Busch, W., Andersen, S. U., Jeong, S., Lohmann, J. U. and Schneitz, K. (2009). *DETORQUEO*, *QUIRKY*, and *ZERZAUST* represent novel components involved in organ development mediated by the receptor-like kinase STRUBBELIG in *Arabidopsis thaliana*. *PLoS Genet.* **5**, e1000355.

Gaudioso-Pedraza, R. and Benitez-Alfonso, Y. (2014). A phylogenetic approach to study the origin and evolution of plasmodesmata-localized glycosyl hydrolases family 17. *Front. Plant Sci.* **5**, 212.

Gillmor, C. S., Lukowitz, W., Brininstool, G., Sedbrook, J. C., Hamann, T., Poindexter, P. and Somerville, C. (2005). Glycosylphosphatidylinositol-anchored proteins are required for cell wall synthesis and morphogenesis in Arabidopsis. *Plant Cell* **17**, 1128-1140.

Gross-Hardt, R., Lenhard, M. and Laux, T. (2002). *WUSCHEL* signaling functions in interregional communication during *Arabidopsis* ovule development. *Genes Dev.* **16**, 1129-1138.

Han, X., Hyun, T. K., Zhang, M., Kumar, R., Koh, E. J., Kang, B.-H., Lucas, W. J. and Kim, J. Y. (2014). Auxin-callose-mediated plasmodesmal gating is essential for tropic auxin gradient formation and signaling. *Dev. Cell* **28**, 132-146.

Hejatko, J., Blilou, I., Brewer, P. B., Friml, J., Scheres, B. and Benkova, E. (2006). In situ hybridization technique for mRNA detection in whole mount Arabidopsis samples. *Nat. Protoc.* **1**, 1939-1946.
Henrissat, B., Coutinho, P. M. and Davies, G. J. (2001). A census of carbohydrate-active enzymes in the genome of *Arabidopsis thaliana*. *Plant Mol. Biol.* **47**, 55-72.
Koncz, C. and Schell, J. (1986). The promoter of TL-DNA gene 5 controls the tissue-specific expression of chimaeric genes carried by a novel Agrobacterium binary vector. *Mol. Gen. Genet.* **204**, 383-396.
Kwak, S.-H. and Schiefelbein, J. (2008). A feedback mechanism controlling SCRAMBLED receptor accumulation and cell-type pattern in *Arabidopsis*. *Curr. Biol.* **18**, 1949-1954.
Kwak, S.-H., Shen, R. and Schiefelbein, J. (2005). Positional signaling mediated by a receptor-like kinase in *Arabidopsis*. *Science* **307**, 1111-1113.
Kwak, S.-H., Woo, S., Lee, M. M. and Schiefelbein, J. (2014). Distinct signaling mechanisms in multiple developmental pathways by the SCRAMBLED receptor of Arabidopsis. *Plant Physiol.* **166**, 976-987.
Le Roy, K., Vergauwen, R., Struyf, T., Yuan, S., Lammens, W., Mátrai, J., De Maeyer, M. and Van den Ende, W. (2013). Understanding the role of defective invertases in plants: tobacco Nin88 fails to degrade sucrose. *Plant Physiol.* **161**, 1670-1681.
Leubner-Metzger, G. and Meins, F. J. (1999). Functions and regulation of plant beta-1,3-glucanases (PR-2). In *Pathogenesis-Related Proteins in Plants* (ed. S. K. Datta and S., Muthukrishan), pp. 49-76. Boca Raton, FL: CRC Press.
Levy, A., Erlanger, M., Rosenthal, M. and Epel, B. L. (2007). A plasmodesmata-associated beta-1,3-glucanase in Arabidopsis. *Plant J.* **49**, 669-682.
Li, C., Yeh, F. L., Cheung, A. Y., Duan, Q., Kita, D., Liu, M. C., Maman, J., Luu, E. J., Wu, B. W., Gates, L. et al. (2015). Glycosylphosphatidylinositol-anchored proteins as chaperones and co-receptors for FERONIA receptor kinase signaling in Arabidopsis. *Elife* **4**, doi: 10.7554/eLife.06587.
Lin, L., Zhong, S.-H., Cui, X.-F., Li, J. and He, Z.-H. (2012). Characterization of temperature-sensitive mutants reveals a role for receptor-like kinase SCRAMBLED/STRUBBELIG in coordinating cell proliferation and differentiation during Arabidopsis leaf development. *Plant J.* **72**, 707-720.
Liu, L., Shang-Guan, K., Zhang, B., Liu, X., Yan, M., Zhang, L., Shi, Y., Zhang, M., Qian, Q., Li, J. et al. (2013). Brittle Culm1, a COBRA-like protein, functions in cellulose assembly through binding cellulose microfibrils. *PLoS Genet.* **9**, e1003704.
Liu, X., Castro, C., Wang, Y., Noble, J., Ponvert, N., Bundy, M., Hoel, C., Shpak, E. and Palanivelu, R. (2016). The role of LORELEI in pollen tube reception at the interface of the synergid cell and pollen tube requires the modified eight-cysteine motif and the receptor-like kinase FERONIA. *Plant Cell* **28**, 1035-1052.
Lu, P., Porat, R., Nadeau, J. A. and O'Neill, S. D. (1996). Identification of a meristem L1 layer-specific gene in Arabidopsis that is expressed during embryonic pattern formation and defines a new class of homeobox genes. *Plant Cell* **8**, 2155-2168.
Mayer, K. F. X., Schoof, H., Haecker, A., Lenhard, M., Jürgens, G. and Laux, T. (1998). Role of *WUSCHEL* in regulating stem cell fate in the *Arabidopsis* shoot meristem. *Cell* **95**, 805-815.
Orlean, P. and Menon, A. K. (2007). Thematic review series: lipid posttranslational modifications. GPI anchoring of protein in yeast and mammalian cells, or: how we learned to stop worrying and love glycophospholipids. *J. Lipid Res.* **48**, 993-1011.
Otero, S., Helariutta, Y. and Benitez-Alfonso, Y. (2016). Symplastic communication in organ formation and tissue patterning. *Curr. Opin. Plant Biol.* **29**, 21-28.
Oxley, D. and Bacic, A. (1999). Structure of the glycosylphosphatidylinositol anchor of an arabinogalactan protein from *Pyrus communis* suspension-cultured cells. *Proc. Natl. Acad. Sci. USA* **96**, 14246-14251.
Pierleoni, A., Martelli, P. L. and Casadio, R. (2008). PredGPI: a GPI-anchor predictor. *BMC Bioinformatics* **9**, 392.
Ranf, S., Grimmer, J., Pöschl, Y., Pecher, P., Chinchilla, D., Scheel, D. and Lee, J. (2012). Defense-related calcium signaling mutants uncovered via a quantitative high-throughput screen in *Arabidopsis thaliana*. *Mol. Plant* **5**, 115-130.
Rinne, P. L. H., Welling, A., Vahala, J., Ripel, L., Ruonala, R., Kangasjärvi, J. and van der Schoot, C. (2011). Chilling of dormant buds hyperinduces *FLOWERING LOCUS T* and recruits GA-inducible 1,3-beta-glucanases to reopen signal conduits and release dormancy in *Populus*. *Plant Cell* **23**, 130-146.
Roudier, F., Fernandez, A. G., Fujita, M., Himmelspach, R., Borner, G. H., Schindelman, G., Song, S., Baskin, T. I., Dupree, P., Wasteneys, G. O. et al. (2005). COBRA, an Arabidopsis extracellular glycosyl-phosphatidyl inositol-anchored protein, specifically controls highly anisotropic expansion through its involvement in cellulose microfibril orientation. *Plant Cell* **17**, 1749-1763.
Schneitz, K., Hülskamp, M. and Pruitt, R. E. (1995). Wild-type ovule development in *Arabidopsis thaliana*: a light microscope study of cleared whole-mount tissue. *Plant J.* **7**, 731-749.
Schneitz, K., Hülskamp, M., Kopczak, S. D. and Pruitt, R. E. (1997). Dissection of sexual organ ontogenesis: a genetic analysis of ovule development in *Arabidopsis thaliana*. *Development* **124**, 1367-1376.
Schultz, C. J., Johnson, K. L., Currie, G. and Bacic, A. (2000). The classical arabinogalactan protein gene family of Arabidopsis. *Plant Cell* **12**, 1751-1768.
Sessions, A., Weigel, D. and Yanofsky, M. F. (1999). The *Arabidopsis thaliana MERISTEM LAYER1* promoter specifies epidermal expression in meristems and young primordia. *Plant J.* **20**, 259-263.
Sieber, P., Gheyeselinck, J., Gross-Hardt, R., Laux, T., Grossniklaus, U. and Schneitz, K. (2004). Pattern formation during early ovule development in *Arabidopsis thaliana*. *Dev. Biol.* **273**, 321-334.
Sieburth, L. E. and Meyerowitz, E. M. (1997). Molecular dissection of the *AGAMOUS* control region shows that *cis* elements for spatial regulation are located intragenically. *Plant Cell* **9**, 355-365.
Simpson, C., Thomas, C., Findlay, K., Bayer, E. and Maule, A. J. (2009). An Arabidopsis GPI-anchor plasmodesmal neck protein with callose binding activity and potential to regulate cell-to-cell trafficking. *Plant Cell* **21**, 581-594.
Sundaresan, V., Springer, P., Volpe, T., Haward, S., Jones, J. D., Dean, C., Ma, H. and Martienssen, R. (1995). Patterns of gene action in plant development revealed by enhancer trap and gene trap transposable elements. *Genes Dev.* **9**, 1797-1810.
Tilsner, J., Nicolas, W., Rosado, A. and Bayer, E. M. (2016). Staying tight: plasmodesmal membrane contact sites and the control of cell-to-cell connectivity in plants. *Annu. Rev. Plant Biol.* **67**, 337-364.
Tran, H. T. and Plaxton, W. C. (2008). Proteomic analysis of alterations in the secretome of Arabidopsis thaliana suspension cells subjected to nutritional phosphate deficiency. *Proteomics* **8**, 4317-4326.
Trehin, C., Schrempp, S., Chauvet, A., Berne-Dedieu, A., Thierry, A.-M., Faure, J.-E., Negrutiu, I. and Morel, P. (2013). *QUIRKY* interacts with *STRUBBELIG* and *PAL OF QUIRKY* to regulate cell growth anisotropy during *Arabidopsis* gynoecium development. *Development* **140**, 4807-4817.
Vaddepalli, P., Fulton, L., Batoux, M., Yadav, R. K. and Schneitz, K. (2011). Structure-function analysis of STRUBBELIG, an Arabidopsis atypical receptor-like kinase involved in tissue morphogenesis. *PLoS One* **6**, e19730.
Vaddepalli, P., Herrmann, A., Fulton, L., Oelschner, M., Hillmer, S., Stratil, T. F., Fastner, A., Hammes, U. Z., Ott, T., Robinson, D. G. et al. (2014). The C2-domain protein QUIRKY and the receptor-like kinase STRUBBELIG localize to plasmodesmata and mediate tissue morphogenesis in *Arabidopsis thaliana*. *Development* **141**, 4139-4148.
Yadav, R. K., Fulton, L., Batoux, M. and Schneitz, K. (2008). The *Arabidopsis* receptor-like kinase STRUBBELIG mediates inter-cell-layer signaling during floral development. *Dev. Biol.* **323**, 261-270.
Yu, S., Guo, Z., Johnson, C., Gu, G. and Wu, Q. (2013). Recent progress in synthetic and biological studies of GPI anchors and GPI-anchored proteins. *Curr. Opin. Chem. Biol.* **17**, 1006-1013.
Zapata-Hommer, O. and Griesbeck, O. (2003). Efficiently folding and circularly permuted variants of the Sapphire mutant of GFP. *BMC Biotechnol.* **3**, 5.
Zavaliev, R., Ueki, S., Epel, B. L. and Citovsky, V. (2011). Biology of callose (beta-1,3-glucan) turnover at plasmodesmata. *Protoplasma* **248**, 117-130.
Zavaliev, R., Levy, A., Gera, A. and Epel, B. L. (2013). Subcellular dynamics and role of Arabidopsis beta-1,3-glucanases in cell-to-cell movement of tobamoviruses. *Mol. Plant Microbe Interact.* **26**, 1016-1030.

Supplemental Information

Supplemental Figures

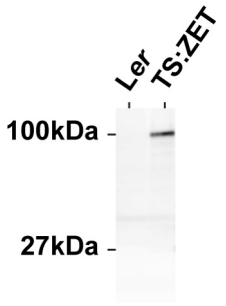

Fig. S1. Western blot using an extract of 6-day *pZET::TS:ZET zet-1* seedlings probed with an anti-GFP antibody. A single band is detected indicating an intact TS:ZET fusion protein. The observed molecular weight of the fusion protein (100 kDa) is larger than the expected one (80 kDa) suggesting posttranslational modification.

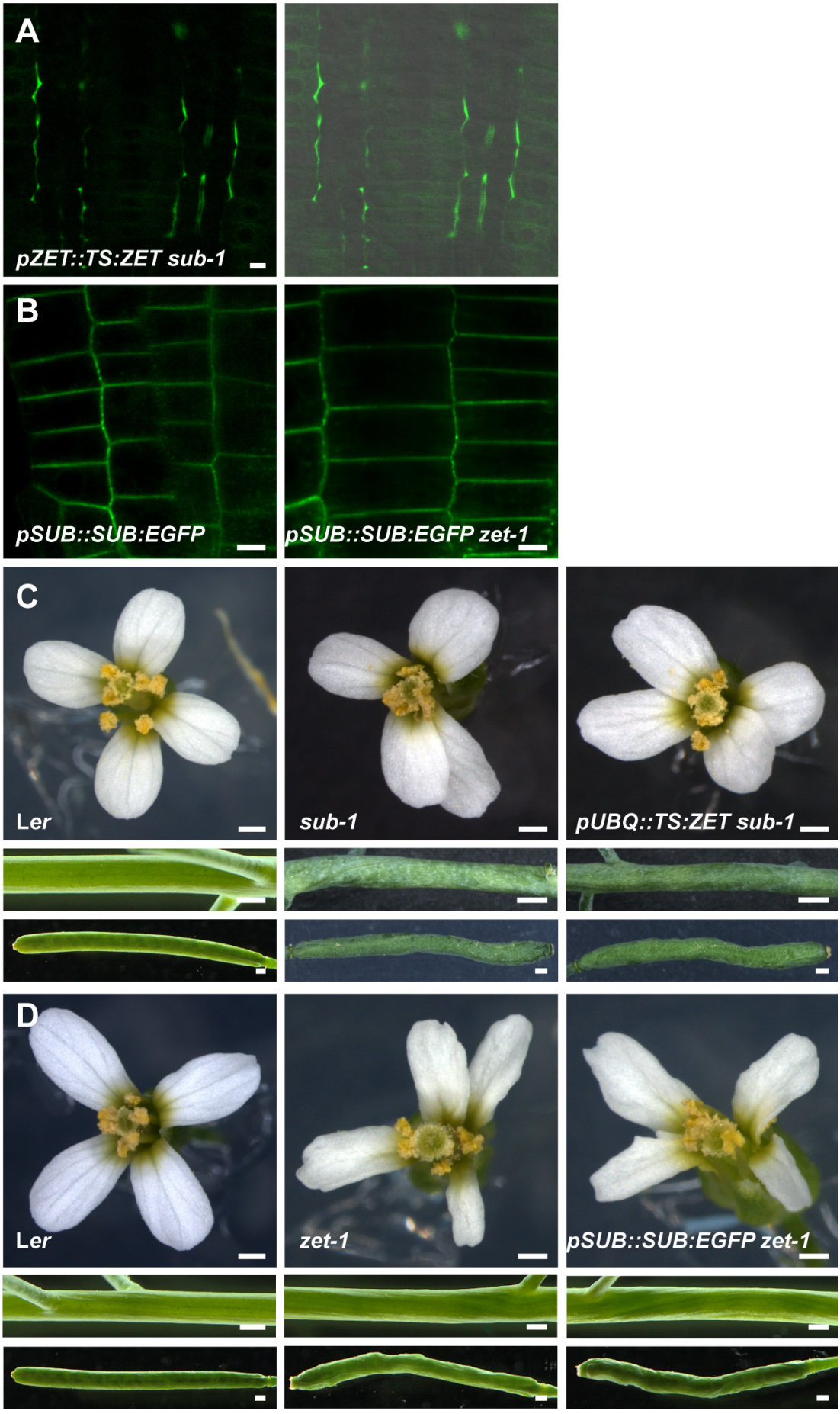

Fig. S2. Analysis of TS:ZET and SUB:EGFP signal localization in different mutant backgrounds. (A) and **(B)** Optical sections through the meristematic region of a 5-day root. **(C)** and **(D)** Upper panels: Stage 13 flower. Middle panel: Siliques. Bottom panel: Stem. Genotypes are indicated. **(A)** Note regular TS:ZET signal distribution in *sub-1* (compare with Fig. 3C). Right panel includes DIC channel. **(B)** The spotty SUB:EGFP signal is identical in wild type (left panel) and *zet-1* (right panel). **(C)** A functional *pUBQ::TS:ZET* transgene does not influence the *sub-1* phenotype. **(D)** A functional *pSUB::SUB:EGFP* transgene does not influence the *zet-1* phenotype. Abbreviations: DIC, differential interference contrast. Scale bars: 10 μm.

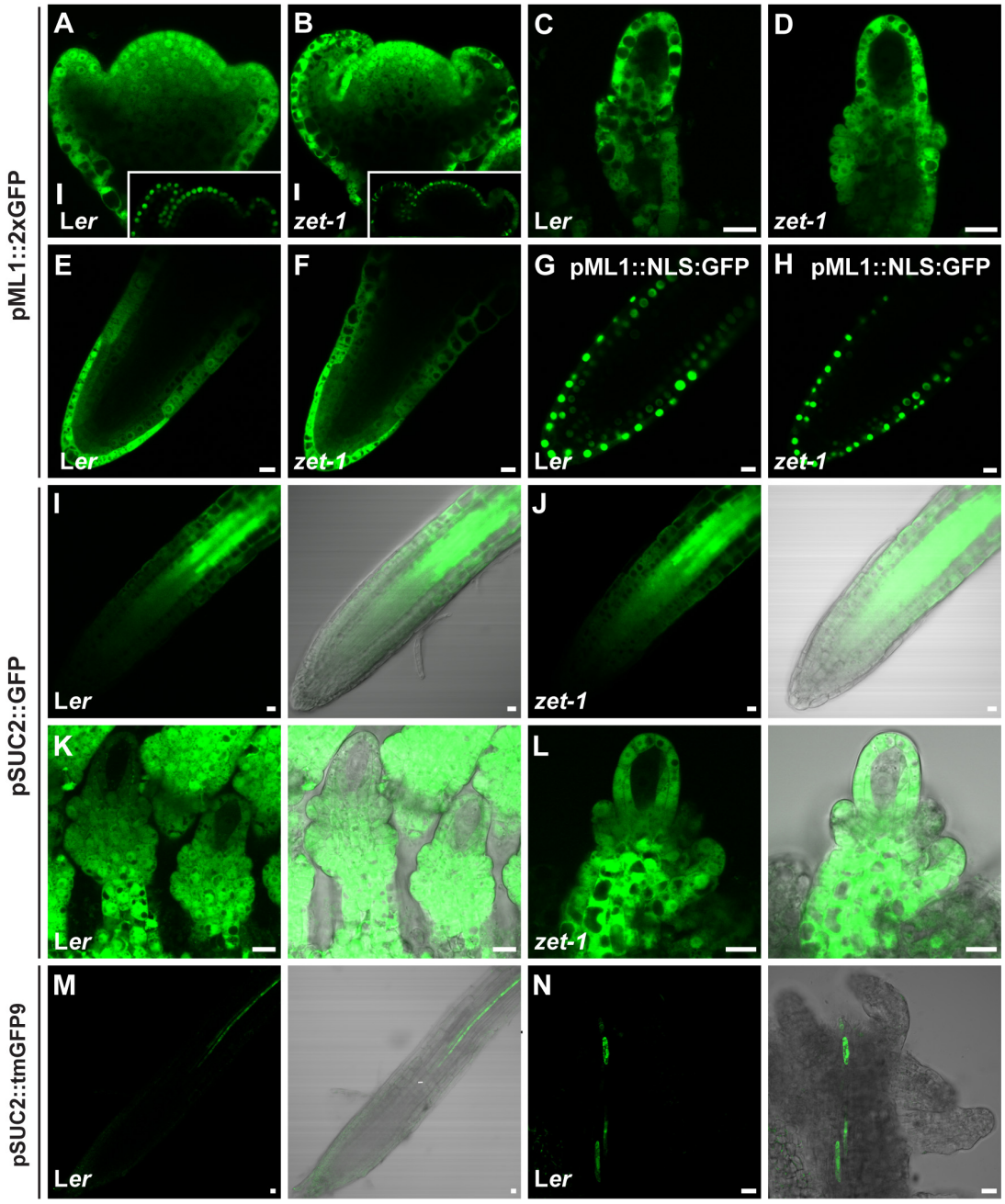

Fig. S3. Inter-cell layer movement of GFP in L*er* and *zet-1*. Longitudinal confocal micrographs of tissue expressing the pML1::2xGFP or pSUC2::GFP reporters, respectively. Genotypes are indicated. (**A**) and (**B**) Stage 3 floral meristems, (**C**) and (**D**), (**K**) and (**L**) Stage 2-III ovules. (**E**) to (**H**) Lateral root tip of 10-day seedling. (**I**) and (**J**), (**M**) Main root tip of 5-day seedling. (**N**) Stage 11 carpel tissue showing placenta and young stage 2-III ovules. (**A**) to (**F**) Free 2xGFP expression driven by the epidermis-specific *ML1* promoter. The diffuse gradient of GFP signal intensity

indicates movement of GFP from the epidermis to sub-epidermal tissue. Signal distribution does not noticeably differ between genotypes. **(A)** and **(B)** Note the epidermis-restricted localization of a nuclear pML1::NLS:GFP reporter (insets). (**G**) and (**H**), Control using a nuclear localized GFP reporter (pML1::NLS:GFP). Note epidermis-specific signal. **(H)** Different optical section from root depicted in Fig. 6B. (**I**) to (**L**) Left panels: confocal micrographs, right panels: overlay with DIC channel. Free GFP expression driven by the *SUC2* promoter. Note unaltered diffusion from the metaphloem companion cells to the lateral cell layers. (**M**) and (**N**), The *SUC2* promoter drives expression of a membrane-anchored GFP (tmGFP9). Signal marks the expression domain of the *SUC2* promoter in companion cells of the metaphloem. Abbreviations: DIC, differential interference contrast. Scale bars: 10 µm.

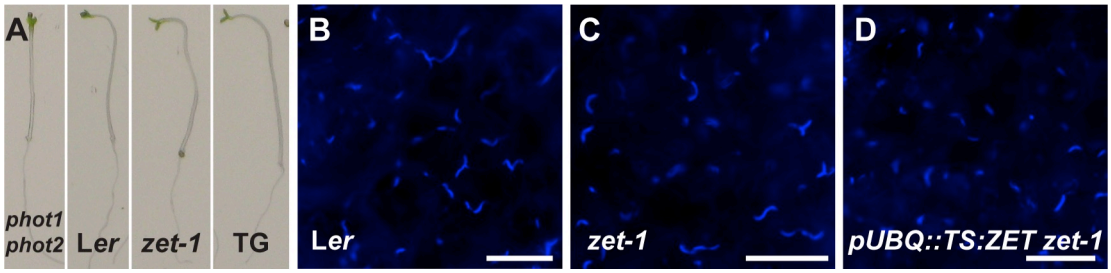

Fig. S4. Phototropism and callose deposition assays. (**A**) Phototropism assay. 3-days-old dark-grown seedlings were illuminated with blue light coming from the left. The *phot1 phot2* control plants lack the blue light receptor responsible for phototropism and are defective in the photropism response (Christie et al., 1998). TG: *pUBQ::TS:ZET zet-1*. Phototropism appears normal in plants with altered *ZET* activity. (**B**) to (**D**) Cotyledon epidermis. Callose deposition upon addition of 1 µM flg22 appears unaltered in plants with altered *ZET* activity. Scale bars: 50 µm.

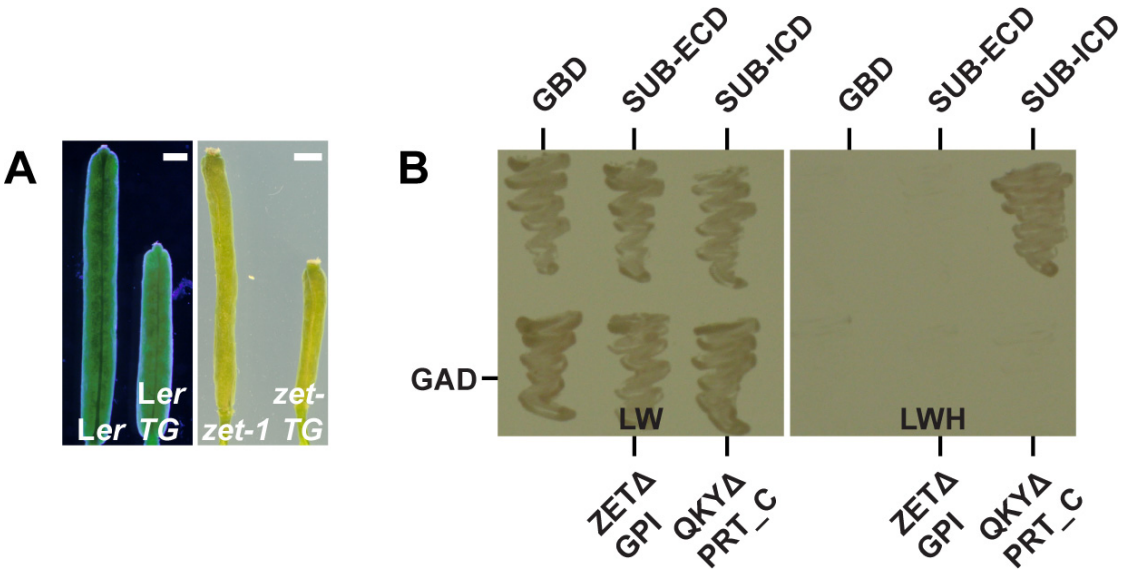

Fig. S5. Analysis of *SUB* and *ZET* interactions. (A) Plants ectopically expressing *SUB:EGFP* in L*er* or *zet-1* exhibit comparably shorter siliques. Genotypes are indicated. Abbreviations: TG: *pUBQ::SUB:EGFP*. Scale bars: 1 mm. **(B)** Yeast two-hybrid assay involving a ZET variant lacking the GPI anchor addition domain (ZETΔGPI), a QKY variant, including all four C2 domains but lacking the PRT_C domain (QKYΔPRT_C) fused to the GAL4 activating domain (GAD) and the extracellular domain (ECD) or intracellular domain (ICD) of SUB fused to the GAL4 DNA-binding domain (GBD), respectively (Vaddepalli et al., 2014). Growth on –LW panel indicates successful transformation of both plasmids and on –LWH panel indicates presence or absence of interaction.

Supplemental Tables

Table S1. Summary of *zet* alleles.

Allele	Mutagen	Mutation#	Amino acid change/transcript	Background	Reference
zet-1	EMS	T>Δ, 265	S88--*	L*er*	this study Fulton et. al. 2009
zet-2	T-DNA Ds Transposon-ET13436	193/LB	M64--*	L*er*	this study

#the coordinates refer to the genomic sequence and relate to the ATG of *ZET* (At1g64760).
--*indicates various aberrant sequences of residues followed by a stop.

Table S2. Primers used in this study.

Primer Name	Sequence (5'-3')
CER453151_F	GCTCTGTTAGGTACGCCTTTTGTTACAAAC
CER453151_R	GTGAGTAACGTGCATGTTGTTGGAATC
F13011_F	AGTGATTGGATGGTCGGTATG
F13011_R	TGGTTTTGGTGAGTTCTGCT
530(TaqI)_F	TCTGAATCTGAAACCACGACCAAGG
530(TaqI)_R	GGAGTCCACTCAGGTAACTTTTTCC
840(ClaI)_F	GCTGATGTATTGGATTTGAGTCGGT
840(ClaI)_R	AAGCCGAAGAGCCACAACAGGAAAT
ZETsense_Insitu_F	TAATACGACTCACTATAGGGTTCCCCAAAACCAAAA AGTTTAC
ZETsense_InsituM_R	ATCTGTAAGCACTGCCTGCATTA
ZETas_Insitu_F	TTCCCCAAAACCAAAAAGTTTAC
ZETas_InsituM_R	TAATACGACTCACTATAGGGATCTGTAAGCACTGCC TGCATTA
EGFP_sense_F	TAATACGACTCACTATAGGGGTCGAGCTGGACGGC GACGT
EGFP_sense_R	GCGCTTCTCGTTGGGGTCTTTGCTCAGGG
EGFP_as_F	GTCGAGCTGGACGGCGACGT
EGFP_as_R	TAATACGACTCACTATAGGGGCGCTTCTCGTTGGGG TCTT
PDCB1_EcoRI_F	CCGAATTCTGGTGTGTGTGTAAGACAGGGC
PDCB1_Xho1_R	TGCTCGAGGCTGTCTGTCGTGTAATCCGGG
ZETGH_EcoRI_F	CCGAATTCTTGGGTGTGAATTGGGGAACAA
ZETX8_XhoI_R	TGCTCGAGATTGCATTGTCCTTGAGATATA
ZET_Entry clone_F_KpnI	TAGGTACCATGTCGAATCTGTTGGCTC TC
ZET_Entryclone_R_ XhoI	TAGACTCGAGTCAAAACATCATCCCTGATAAC
ZET_NdeI_F (Y2H)	TGCATATGTTGGGTGTGAATTGGGGAAC
ZET_EcoRI_R (Y2H)	GAGAATTCATTGCATTGTCCTTGAGATA
ZETpro_F	ATGAGCTCTGATGGAGAGTAAGGAGAGG
ZETpro_R	TAACCGGTCGATTTTCACCTGAGAAAGAT
ZET_EcoRI_F	AGTGAATTCTTGGGTGTGAATTGGGGAA
ZET_BamHI_R	TCAAGGACAATGCAATTTCCGGATCCAT
ZET F448*_F	CAAGGACAATGCAATTGACCTATTCAGATTGTGG
ZET F448*_R	CCACAATCTGAATAGGTCAATTGCATTGTCCTTG

Supplemental Materials and Methods

Map-Based Cloning of *ZET*

To map the *ZET* locus at high resolution, an F2-mapping population was generated by outcrossing *zet-1* (L*er*) to wild-type (Col). The F2 progeny were screened for *zet* individuals based on twisted inflorescence morphology. Genomic DNA was isolated and used for PCR-based amplification of molecular markers. The *zet-1* mutation was initially mapped to a single region on the lower arm of chromosome 1 between markers CER453151 and F13011. Further fine-mapping placed *zet-1* in a 138 kb interval between the two CAPS markers 530(TaqI) and 840(ClaI). Candidate genes were analyzed by T-DNA insertion mutant analysis and/or sequence determination revealing that *zet-1* carries a mutation in At1g64760. A second *zet* mutant carrying a mutation in At1g64760 (*zet-2*) was identified in the Cold Spring Harbor GeneTrap Ds-transposon insertion line collection (Sundaresan et al., 1995). Finally, the mutant *zet-1* phenotype could be fully complemented by a construct encoding a T-Sapphire:ZET fusion protein driven by the native *ZET* promoter (pZET::TS:ZET) (Fig. 1).

Supplemental References

Christie, J. M., Reymond, P., Powell, G. K., Bernasconi, P., Raibekas, A. A., Liscum, E. and Briggs, W. R. (1998). Arabidopsis NPH1: a flavoprotein with the properties of a photoreceptor for phototropism. *Science* **282**, 1698-1701.

Sundaresan, V., Springer, P., Volpe, T., Haward, S., Jones, J. D., Dean, C., Ma, H. and Martienssen, R. (1995). Patterns of gene action in plant development revealed by enhancer trap and gene trap transposable elements. *Genes Dev* **9**,

1797-1810.

Vaddepalli, P., Herrmann, A., Fulton, L., Oelschner, M., Hillmer, S., Stratil, T. F., Fastner, A., Hammes, U. Z., Ott, T., Robinson, D. G. et al. (2014). The C2-domain protein QUIRKY and the receptor-like kinase STRUBBELIG localize to plasmodesmata and mediate tissue morphogenesis in *Arabidopsis thaliana*. *Development* **141**, 4139-4148.